PERGAMON

International Journal of Solids and Structures 36 (1999) 3945–3976

INTERNATIONAL JOURNAL OF SOLIDS and STRUCTURES

Design and fabrication of submerged cylindrical laminates—II. Effect of fiber pre-stress

Mullahalli V. Srinivas[a], George J. Dvorak[a,*], Petr Prochazka[b]

[a] *Center for Composite Materials and Structures, Rensselaer Polytechnic Institute, Troy, NY 12180-3590, U.S.A.*
[b] *Department of Structural Mechanics, Faculty of Civil Engineering, Czech Technical University, Prague, Czech Republic*

Received 21 August 1997; in revised form 5 June 1998

Abstract

This is the sequel to the first part of this paper (Dvorak et al., 1999, Int. J. Solids Structures 36, 3917–3943), concerned with modeling and analysis of laminated composite cylinder fabrication procedures, such as filament winding or fiber placement, which involve fiber pre-stress for waviness reduction as well as overall or local heating to and cooling from matrix curing temperatures. The fiber pre-stress applied in individual plies is shown to cause a self-stress in the respective plies, and relaxation stresses in the already completed plies and in the supporting mandrel. The final residual stress state is reached after mandrel removal. Influence functions that relate the ply stresses to the applied pre-stress forces are derived. Direct problems are solved for ply stresses caused by prescribed constant or linearly or parabolically changing pre-stress magnitudes in the layers. A superposition of the constant and parabolic distributions is shown to lead to nearly uniform stresses through the cylinder wall. The magnitudes depend on the radial stiffness of the mandrel that supports the structure during fabrication. Inverse problems are formulated as nonlinear optimizations and solved by quadratic programming. The goal is to determine fiber pre-stress distributions through the wall thickness such that the total stresses due to external hydrostatic pressure and fiber pre-stress are as uniform as possible through the wall thickness and confined by the ply strength magnitudes.

1. Introduction

It is well known that relatively thick unidirectional fiber composites that are carefully manufactured for reduced fiber waviness and low matrix porosity can support axial compressive stresses of significant magnitudes (Daniel and Isahi, 1994). In large structures that are produced by fiber placement or filament winding, fiber waviness can be reduced by fiber pre-stress applied prior to curing. Relatively small forces are needed, for example a 113 lb force is shown to cause a 1000

* Corresponding author. Fax: 001 518 276; e-mail: dvorak@rpi.edu

0020–7683/99/$ - see front matter
PII: S0020–7683(98)00182–6

MPa pre-stress in a typical 10,000 filament tow. However, apart from the potentially beneficial effect on ply compressive strength, the consequences of fiber pre-stress applied in a large laminated structure are not well understood.

This paper examines the residual stresses caused by fiber pre-stress applied in individual plies during fabrication of a laminated cylindrical structure. Using the theoretical framework developed in Part I (Dvorak et al., 1999) we establish in Section 2 a set of influence functions that evaluate the ply residual stresses in terms of the pre-stress forces applied to the individual layers of the laminate. We also examine the effect of cooling from the curing temperature on the residual stress state and show that very different residual states can be caused by either overall heating and cooling of the entire cylinder, or by local heating applied in fiber placement procedures. Then, in Section 3, ply residual stresses are found for certain prescribed distribution of fiber pre-stress magnitudes through the cylinder wall thickness. In particular, constant pre-stress applied uniformly to all plies is shown to produce possibly high stress gradients, with compressive stresses at the inner surface that may impair the load bearing capacity of the structure. More favorable, nearly uniform residual stresses are found in the cylinder wall with variable pre-stress distributions. Finally, Section 4 presents a nonlinear optimization procedure for solving the inverse problem of finding fiber pre-stress distribution that generates minimized residual stresses that do not exceed certain prescribed magnitudes. In superposition with the stresses due to the applied hydrostatic pressure, the residuals produce total stresses that lie within given ply strength limits. The desirable pre-stress distribution is found to depend, in part, on the stiffness of the mandrel that supports the composite structure during fabrication.

2. Model of the fabrication process

The fabrication procedure model adopted here applies to a cylindrical laminated structure laid up in successive layers on an elastic mandrel of certain radial and axial stiffness. Fiber placement with in situ curing, or lay-up and curing of either new layers on already cured layers, or of all layers at once, can be represented by the model. As in Part I, Section 2, each layer is assumed to be a cylindrically orthotropic elastic solid with known elastic moduli representing a single ply of certain orientation, or the mandrel. In the analysis, the mandrel is denoted as layer $i = 1$, and the laminate layers as $i = 2, 3, \ldots, N$.

During curing, the fibers in the composite layers are pre-stressed at the curing temperature by a certain force P_i. This force can be resolved into its components in the cylinder hoop and axial directions as P_i^θ and P_i^z, respectively. The P_i^θ/P_i^z ratio depends on the angle that the helix trajectory of the fiber contains with the cylinder axis. After all the layers have been laid, the mandrel is removed, leaving a $(N-1)$ layered cylindrical laminate.

During the fabrication process, initial strains are introduced by the pre-stress forces and by cooling of the layers from the curing temperature, hence residual stresses are generated in the structure as it is built up on the mandrel. At completion of the fabrication process, the mandrel itself supports certain radial traction force R and a total axial force Z. After mandrel removal, the residual stress state is changed by superposition with stresses caused by internal radial force $-R$ and axial force $-Z$.

In what follows, the respective contributions to the final residual stress state will be evaluated

in terms of stress averages in the layers. The self-stress caused by fiber pre-stress will be denoted by $\langle\boldsymbol{\sigma}\rangle^{\alpha}$, the relaxation stress in the existing layers due to tractions imposed by pre-stressing the current layer by $\langle\boldsymbol{\sigma}\rangle^{\beta}$, the superposition of these stresses that describes the stress state in the completed structure prior to mandrel removal by $\langle\boldsymbol{\sigma}\rangle^{\gamma}$, and the stresses induced by mandrel removal by $\langle\boldsymbol{\sigma}\rangle^{\delta}$. The superposition of the last two states provides the final residual stress distribution in the structure.

2.1. Self-stress

As in Part I, Section 2, consider a cylindrical layer (i) of inner radius a_i, outer radius b_i and thickness $t_i = b_i - a_i$. Let ψ_i denote the angle that all fibers in the layer (i) contain with the longitudinal z-axis of the cylinder. The self-stress $\langle\sigma^i\rangle^{\alpha}$ in layer (i) is caused by application of a certain pre-stress force P_i to each fiber in its winding direction ψ_i, both before and during curing; therefore, this stress is preserved after curing as part of the total fiber stress. The fiber pre-stress force components in the hoop and axial directions are,

$$P_i^{\theta} = P_i \sin\psi \qquad P_i^{z} = P_i \cos\psi \tag{1}$$

The axial and hoop components of the self-stress in the cylinder coordinate system of Fig. 1 of Part I (Dvorak et al., 1999) can be found as follows. Consider a small square element of the ith layer in the θz-plane, where the θ-axis is in the hoop direction and z-axis in the longitudinal direction of the composite cylinder. For simplicity, let the reinforcement be represented by a monolayer of fibers of diameter d_f^i and spacing s_i, evaluated in terms of fiber volume fraction c_f^i as,

$$s_i = \frac{\pi (d_f^i)^2}{4 t_i c_f^i} \tag{2}$$

This represents the average distance between the fiber axes measured in the direction perpendicular to the fibers in each ply. However, in the planes perpendicular to the θ- and z-axes of the cylinder, the average distances between the fiber axes will be,

$$s_z^i = \frac{s_i}{\sin\psi_i} \quad \text{on planes } \theta = \text{const.} \tag{3}$$

$$s_\theta^i = \frac{s_i}{\cos\psi_i} \quad \text{on planes } z = \text{const.} \tag{4}$$

Since the force P_i are applied to the individual fibers, the hoop and axial components of the self-stress $\langle\sigma^i\rangle^{\alpha}$ are related to the force components (1) as,

$$\langle\sigma_{\theta\theta}^i\rangle^{\alpha} = \frac{P_i^{\theta}}{s_z^i t_i} \tag{5}$$

$$\langle\sigma_{zz}^i\rangle^{\alpha} = \frac{P_i^{z}}{s_\theta^i t_i} \tag{6}$$

Substituting for (1)–(4) eliminates the auxiliary parameters s_i and t_i and provides the self-stress components in the form:

$$\langle\sigma^i_{\theta\theta}\rangle^\alpha = \frac{4c^i_f P_i \sin^2\psi_i}{\pi(d^i_f)^2} \qquad \langle\sigma^i_{zz}\rangle^\alpha = \frac{4c^i_f P_i \cos^2\psi_i}{\pi(d^i_f)^2} \tag{7}$$

where the expression $4P_i/(\pi(d^i_f)^2)$ represents the magnitude of the actual pre-stress applied to the fibers. Note that $\langle\sigma^i_{\theta\theta}\rangle^\alpha = 0$ for 0° plies, $\langle\sigma^i_{zz}\rangle^\alpha = 0$ for 90° plies and $\langle\sigma^i_{\theta\theta}\rangle^\alpha = 3\langle\sigma^i_{zz}\rangle^\alpha$ for 60° plies.

Let the hoop and axial stress averages in each layer be expressed as

$$\boldsymbol{\sigma}^\alpha_{\theta\theta} = [\langle\sigma^2_{\theta\theta}\rangle^\alpha, \langle\sigma^3_{\theta\theta}\rangle^\alpha, \langle\sigma^4_{\theta\theta}\rangle^\alpha, \ldots, \langle\sigma^N_{\theta\theta}\rangle^\alpha]^T \tag{8}$$

$$\boldsymbol{\sigma}^\alpha_{zz} = [\langle\sigma^2_{zz}\rangle^\alpha, \langle\sigma^3_{zz}\rangle^\alpha, \langle\sigma^4_{zz}\rangle^\alpha, \ldots, \langle\sigma^N_{zz}\rangle^\alpha]^T \tag{9}$$

Substituting for the stress components in (8) and (9) from (7) and (8)

$$\boldsymbol{\sigma}^\alpha_{\theta\theta} = \boldsymbol{S}^\alpha_{\theta\theta}\boldsymbol{P}^\theta + \boldsymbol{S}^\alpha_{\theta z}\boldsymbol{P}^z \qquad \boldsymbol{\sigma}^\alpha_{zz} = \boldsymbol{S}^\alpha_{z\theta}\boldsymbol{P}^\theta + \boldsymbol{S}^\alpha_{zz}\boldsymbol{P}^z \tag{10}$$

where

$$\boldsymbol{P}^\theta = [P^\theta_2, P^\theta_3, P^\theta_4, \ldots, P^\theta_N]^T \qquad \boldsymbol{P}^z = [P^z_2, P^z_3, P^z_4, \ldots, P^z_N]^T \tag{11}$$

are the $[(N-1)\times 1]$ pre-stressing force vectors in the θ and z directions, respectively. The $\boldsymbol{S}^\alpha_{\theta\theta}$, $\boldsymbol{S}^\alpha_{\theta z}$, $\boldsymbol{S}^\alpha_{z\theta}$ and $\boldsymbol{S}^\alpha_{zz}$ are $[(N-1)\times(N-1)]$ matrices that represent the self-stress influence functions,

$$\boldsymbol{S}^\alpha_{\theta\theta} = \begin{bmatrix} \frac{4c^2_f \sin\psi_2}{\pi(d^2_f)^2} & 0 & 0 & \ldots & 0 \\ 0 & \frac{4c^3_f \sin\psi_3}{\pi(d^3_f)^2} & 0 & \ldots & 0 \\ 0 & 0 & \frac{4c^4_f \sin\psi_4}{\pi(d^4_f)^2} & \ldots & 0 \\ \vdots & \vdots & \vdots & \ddots & \vdots \\ 0 & 0 & 0 & \ldots & \frac{4c^N_f \sin\psi_N}{\pi(d^N_f)^2} \end{bmatrix} \tag{12}$$

$$\boldsymbol{S}^\alpha_{zz} = \begin{bmatrix} \frac{4c^2_f \cos\psi_2}{\pi(d^2_f)^2} & 0 & 0 & \ldots & 0 \\ 0 & \frac{4c^3_f \cos\psi_3}{\pi(d^3_f)^2} & 0 & \ldots & 0 \\ 0 & 0 & \frac{4c^4_f \cos\psi_4}{\pi(d^4_f)^2} & \ldots & 0 \\ \vdots & \vdots & \vdots & \ddots & \vdots \\ 0 & 0 & 0 & \ldots & \frac{4c^N_f \cos\psi_N}{\pi(d^N_f)^2} \end{bmatrix} \tag{13}$$

$$\boldsymbol{S}^{\alpha}_{\theta z} = \boldsymbol{S}^{\alpha}_{z\theta} = \mathbf{0} \tag{14}$$

2.1.1. Thermal stress as part of self-stress

Thermal stresses are created in the structure, for example, by cooling from the curing temperature. In the case of a large structure fabricated by in situ fiber placement involving only local temperature changes, the thermal stresses can be evaluated and included as part of the self-stress. Consider a process where a new layer (j) is laid on already cured ($j-1$) layered cylinder. If a fiber tow being laid is free to contract during cooling, the thermal strain would be

$$\Delta\varepsilon^{f}_{jA} = \alpha^{f}_{jA}\Delta T \tag{15}$$

where α^{f}_{jA} is the axial thermal expansion coefficient of the fiber and ΔT the temperature change. However, the free contraction is restrained by the ($j-1$) layered cylinder. Assuming that the already cured cylinder is rigid enough to completely restrain the radial and axial contraction the pre-stressing force due to the temperature change is,

$$\Delta P^{j}_{t} = \frac{\pi(d^{j}_{f})^2}{4} E^{f}_{jA}\Delta\varepsilon^{f}_{jA} \tag{16}$$

where E^{f}_{jA} is the axial Young's modulus of the fiber. In the fiber placement process, this force is added to the pre-stressing force vectors (11).

If filament winding or wet lay-up are used together with curing of some or all layers, the partially or entirely completed structure undergoes thermal cycling that creates a uniform thermal change in the fabricated layers. As shown in the first part (Dvorak et al., 1999, Section 7), the thermal stresses are not very high, hence cyclic elastic response is anticipated. Therefore, while the residual stress state changes with the addition of each layer, the final state is that in the completed cylinder that has been subjected to uniform cooling from a stress-free state at the curing temperature. It is probably obvious that entirely different residual stress fields are caused in a given structure by the different fabrication procedures.

2.2. Relaxation stresses

These stresses are caused in the already cured layers $i = 2, 3, \ldots, (j-1)$ by applying the pre-stressing forces P_j (Fig. 1) in the layer j. The hoop component of the pre-stressing force P^{θ}_{j} applied a radial traction $\rho^{\circ}_{j}a_j$, where the radial pressure ρ°_{j} can be derived from the equilibrium in the layer (j) as

$$\rho^{\circ}_{j} = \frac{\langle\sigma^{j}_{\theta\theta}\rangle^{\alpha}t_j}{a_j} = \frac{4c^{j}_{f}\langle P^{\theta}_{j}\rangle^{\circ}\sin\psi_j t_j}{\pi(d^{j}_{f})^2 a_j} \tag{17}$$

Similarly, the axial component P^{z}_{j} generates an axial traction $\zeta^{\circ}_{j}\pi(b^2_j - a^2_j)$. The axial stress ζ°_{j} in the new layer (j) is equivalent to the axial self stress $\langle\sigma^{j}_{zz}\rangle^{\alpha}$, therefore,

$$\zeta^{\circ}_{j} = \langle\sigma^{j}_{zz}\rangle^{\alpha} = \frac{4c^{j}_{f}\langle P^{z}_{j}\rangle^{\circ}\cos\psi_j}{\pi(d^{j}_{f})^2} \tag{18}$$

Internal stresses due to unit radial pressure $\rho^{\circ}_{j} = 1$ and unit axial stress $\zeta^{\circ}_{j} = 1$ are first obtained

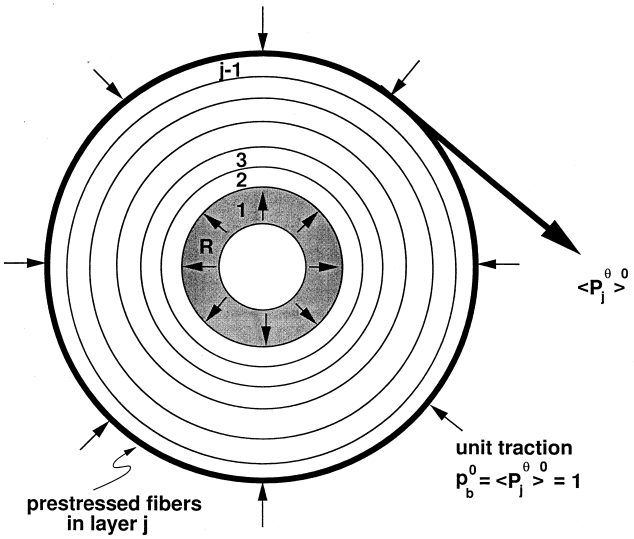

Fig. 1. Stress state during fabrication and fiber pre-stress sequence.

from the solution procedure described by Dvorak et al. (1999). These unit stress solutions are then used to write the hoop and axial stresses in each layer caused by the actual fiber pre-stress forces P_j^θ and P_j^z.

Note that the radial traction and axial force both generate radial, hoop and axial stresses in the layers. The stresses caused by unit radial traction ρ_j° are denoted as $\langle\sigma_{rr}^\rho\rangle_{1,j}^\circ$, $\langle\sigma_{rr}^\rho\rangle_{2,j}^\circ$, $\langle\sigma_{rr}^\rho\rangle_{3,j}^\circ, \ldots, \langle\sigma_{rr}^\rho\rangle_{(j-1),j}^\circ$; $\langle\sigma_{\theta\theta}^\rho\rangle_{1,j}^\circ$, $\langle\sigma_{\theta\theta}^\rho\rangle_{2,j}^\circ$, $\langle\sigma_{\theta\theta}^\rho\rangle_{3,j}^\circ, \ldots, \langle\sigma_{\theta\theta}^\rho\rangle_{(j-1),j}^\circ$; $\langle\sigma_{zz}^\rho\rangle_{1,j}^\circ$, $\langle\sigma_{zz}^\rho\rangle_{2,j}^\circ$, $\langle\sigma_{zz}^\rho\rangle_{3,j}^\circ, \ldots, \langle\sigma_{zz}^\rho\rangle_{(j-1),j}^\circ$.

The stresses caused by the unit axial stress ζ_j° are denoted as, $\langle\sigma_{rr}^\zeta\rangle_{1,j}^\circ$, $\langle\sigma_{rr}^\zeta\rangle_{2,j}^\circ$, $\langle\sigma_{rr}^\zeta\rangle_{3,j}^\circ, \ldots, \langle\sigma_{rr}^\zeta\rangle_{(j-1),j}^\circ$; $\langle\sigma_{\theta\theta}^\zeta\rangle_{1,j}^\circ$, $\langle\sigma_{\theta\theta}^\zeta\rangle_{2,j}^\circ$, $\langle\sigma_{\theta\theta}^\zeta\rangle_{3,j}^\circ, \ldots, \langle\sigma_{\theta\theta}^\zeta\rangle_{(j-1),j}^\circ$; $\langle\sigma_{zz}^\zeta\rangle_{1,j}^\circ$, $\langle\sigma_{zz}^\zeta\rangle_{2,j}^\circ$, $\langle\sigma_{zz}^\zeta\rangle_{3,j}^\circ, \ldots, \langle\sigma_{zz}^\zeta\rangle_{(j-1),j}^\circ$.

The relaxation stresses (denoted by the superscript β) caused in the layers of the completed structure by the actual pre-stressing forces P_j^θ and P_j^z are obtained by superposition of the contributions from pre-stressing of each layer $j = 2, 3,, \ldots, N$

$$\langle\sigma_{rr}^i\rangle^\beta = \sum_{j=i+1}^{N} \left\{ \left[\frac{\langle\sigma_{rr}^\rho\rangle_{i,j}^\circ}{\langle P_j^\theta\rangle^\circ} \right] P_j^\theta + \left[\frac{\langle\sigma_{rr}^\zeta\rangle_{i,j}^\circ}{\langle P_j^z\rangle^\circ} \right] P_j^z \right\} \tag{19}$$

$$\langle\sigma_{\theta\theta}^i\rangle^\beta = \sum_{j=i+1}^{N} \left\{ \left[\frac{\langle\sigma_{\theta\theta}^\rho\rangle_{i,j}^\circ}{\langle P_j^\theta\rangle^\circ} \right] P_j^\theta + \left[\frac{\langle\sigma_{\theta\theta}^\zeta\rangle_{i,j}^\circ}{\langle P_j^z\rangle^\circ} \right] P_j^z \right\} \tag{20}$$

$$\langle\sigma_{zz}^i\rangle^\beta = \sum_{j=i+1}^{N} \left\{ \left[\frac{\langle\sigma_{zz}^\rho\rangle_{i,j}^\circ}{\langle P_j^\theta\rangle^\circ} \right] P_j^\theta + \left[\frac{\langle\sigma_{zz}^\zeta\rangle_{i,j}^\circ}{\langle P_j^z\rangle^\circ} \right] P_j^z \right\} \tag{21}$$

Expressing the hoop and axial relaxation stresses in the vector form

$$\boldsymbol{\sigma}_{\theta\theta}^\beta = [\langle\sigma_{\theta\theta}^2\rangle^\beta, \langle\sigma_{\theta\theta}^3\rangle^\beta, \langle\sigma_{\theta\theta}^4\rangle^\beta, \ldots, \langle\sigma_{\theta\theta}^N\rangle^\beta]^T \tag{22}$$

$$\boldsymbol{\sigma}_{zz}^{\beta} = [\langle \sigma_{zz}^{2} \rangle^{\beta}, \langle \sigma_{zz}^{3} \rangle^{\beta}, \langle \sigma_{zz}^{4} \rangle^{\beta}, \ldots, \langle \sigma_{zz}^{N} \rangle^{\beta}]^{T} \tag{23}$$

and substituting for the stress components $\langle \sigma_{pq}^{i} \rangle^{\beta}$ from (19)–(21) will yield,

$$\boldsymbol{\sigma}_{\theta\theta}^{\beta} = \boldsymbol{S}_{\theta\theta}^{\beta}\boldsymbol{P}^{\theta} + \boldsymbol{S}_{\theta z}^{\beta}\boldsymbol{P}^{z} \qquad \boldsymbol{\sigma}_{zz}^{\beta} = \boldsymbol{S}_{z\theta}^{\beta}\boldsymbol{P}^{\theta} + \boldsymbol{S}_{zz}^{\beta}\boldsymbol{P}^{z} \tag{24}$$

where $\boldsymbol{S}_{\theta\theta}^{\beta}$, $\boldsymbol{S}_{\theta z}^{\beta}$, $\boldsymbol{S}_{z\theta}^{\beta}$ and $\boldsymbol{S}_{zz}^{\beta}$ are the relaxation stress influence functions of dimension $[(N-1)\times(N-1)]$ given by,

$$\boldsymbol{S}_{\theta\theta}^{\beta} = \begin{bmatrix} 0 & \dfrac{\langle \sigma_{\theta\theta}^{\rho} \rangle_{2,3}^{\circ}}{\langle P_{3}^{\theta} \rangle^{\circ}} & \dfrac{\langle \sigma_{\theta\theta}^{\rho} \rangle_{2,4}^{\circ}}{\langle P_{4}^{\theta} \rangle^{\circ}} & \cdots & \dfrac{\langle \sigma_{\theta\theta}^{\rho} \rangle_{2,N-1}^{\circ}}{\langle P_{N-1}^{\theta} \rangle^{\circ}} & \dfrac{\langle \sigma_{\theta\theta}^{\rho} \rangle_{2,N}^{\circ}}{\langle P_{N}^{\theta} \rangle^{\circ}} \\ 0 & 0 & \dfrac{\langle \sigma_{\theta\theta}^{\rho} \rangle_{3,4}^{\circ}}{\langle P_{4}^{\theta} \rangle^{\circ}} & \cdots & \dfrac{\langle \sigma_{\theta\theta}^{\rho} \rangle_{3,N-1}^{\circ}}{\langle P_{N-1}^{\theta} \rangle^{\circ}} & \dfrac{\langle \sigma_{\theta\theta}^{\rho} \rangle_{3,N}^{\circ}}{\langle P_{N}^{\theta} \rangle^{\circ}} \\ \vdots & \vdots & \vdots & \ddots & \vdots & \vdots \\ 0 & 0 & 0 & \cdots & 0 & \dfrac{\langle \sigma_{\theta\theta}^{\rho} \rangle_{N-1,N}^{\circ}}{\langle P_{N}^{\theta} \rangle^{\circ}} \\ 0 & 0 & 0 & \cdots & 0 & 0 \end{bmatrix} \tag{25}$$

$$\boldsymbol{S}_{\theta z}^{\beta} = \begin{bmatrix} 0 & \dfrac{\langle \sigma_{\theta\theta}^{\zeta} \rangle_{2,3}^{\circ}}{\langle P_{3}^{z} \rangle^{\circ}} & \dfrac{\langle \sigma_{\theta\theta}^{\zeta} \rangle_{2,4}^{\circ}}{\langle P_{4}^{z} \rangle^{\circ}} & \cdots & \dfrac{\langle \sigma_{\theta\theta}^{\zeta} \rangle_{2,N-1}^{\circ}}{\langle P_{N-1}^{z} \rangle^{\circ}} & \dfrac{\langle \sigma_{\theta\theta}^{\zeta} \rangle_{2,N}^{\circ}}{\langle P_{N}^{z} \rangle^{\circ}} \\ 0 & 0 & \dfrac{\langle \sigma_{\theta\theta}^{\zeta} \rangle_{3,4}^{\circ}}{\langle P_{4}^{z} \rangle^{\circ}} & \cdots & \dfrac{\langle \sigma_{\theta\theta}^{\zeta} \rangle_{3,N-1}^{\circ}}{\langle P_{N-1}^{z} \rangle^{\circ}} & \dfrac{\langle \sigma_{\theta\theta}^{\zeta} \rangle_{3,N}^{\circ}}{\langle P_{N}^{z} \rangle^{\circ}} \\ \vdots & \vdots & \vdots & \ddots & \vdots & \vdots \\ 0 & 0 & 0 & \cdots & 0 & \dfrac{\langle \sigma_{\theta\theta}^{\zeta} \rangle_{N-1,N}^{\circ}}{\langle P_{N}^{z} \rangle^{\circ}} \\ 0 & 0 & 0 & \cdots & 0 & 0 \end{bmatrix} \tag{26}$$

$$\boldsymbol{S}_{z\theta}^{\beta} = \begin{bmatrix} 0 & \dfrac{\langle \sigma_{zz}^{\rho} \rangle_{2,3}^{\circ}}{\langle P_{3}^{\theta} \rangle^{\circ}} & \dfrac{\langle \sigma_{zz}^{\rho} \rangle_{2,4}^{\circ}}{\langle P_{4}^{\theta} \rangle^{\circ}} & \cdots & \dfrac{\langle \sigma_{zz}^{\rho} \rangle_{2,N-1}^{\circ}}{\langle P_{N-1}^{\theta} \rangle^{\circ}} & \dfrac{\langle \sigma_{zz}^{\rho} \rangle_{2,N}^{\circ}}{\langle P_{N}^{\theta} \rangle^{\circ}} \\ 0 & 0 & \dfrac{\langle \sigma_{zz}^{\rho} \rangle_{3,4}^{\circ}}{\langle P_{4}^{\theta} \rangle^{\circ}} & \cdots & \dfrac{\langle \sigma_{zz}^{\rho} \rangle_{3,N-1}^{\circ}}{\langle P_{N-1}^{\theta} \rangle^{\circ}} & \dfrac{\langle \sigma_{zz}^{\rho} \rangle_{3,N}^{\circ}}{\langle P_{N}^{\theta} \rangle^{\circ}} \\ \vdots & \vdots & \vdots & \ddots & \vdots & \vdots \\ 0 & 0 & 0 & \cdots & 0 & \dfrac{\langle \sigma_{zz}^{\rho} \rangle_{N-1,N}^{\circ}}{\langle P_{N}^{\theta} \rangle^{\circ}} \\ 0 & 0 & 0 & \cdots & 0 & 0 \end{bmatrix} \tag{27}$$

$$\boldsymbol{S}^{\beta}_{zz} = \begin{bmatrix} 0 & \dfrac{\langle\sigma^{\zeta}_{zz}\rangle^{\circ}_{2,3}}{\langle P^{z}_{3}\rangle^{\circ}} & \dfrac{\langle\sigma^{\zeta}_{zz}\rangle^{\circ}_{2,4}}{\langle P^{z}_{4}\rangle^{\circ}} & \cdots & \dfrac{\langle\sigma^{\zeta}_{zz}\rangle^{\circ}_{2,N-1}}{\langle P^{z}_{N-1}\rangle^{\circ}} & \dfrac{\langle\sigma^{\zeta}_{zz}\rangle^{\circ}_{2,N}}{\langle P^{z}_{N}\rangle^{\circ}} \\ 0 & 0 & \dfrac{\langle\sigma^{\zeta}_{zz}\rangle^{\circ}_{3,4}}{\langle P^{z}_{4}\rangle^{\circ}} & \cdots & \dfrac{\langle\sigma^{\zeta}_{zz}\rangle^{\circ}_{3,N-1}}{\langle P^{z}_{N-1}\rangle^{\circ}} & \dfrac{\langle\sigma^{\zeta}_{zz}\rangle^{\circ}_{3,N}}{\langle P^{z}_{N}\rangle^{\circ}} \\ \vdots & \vdots & \vdots & \ddots & \vdots & \vdots \\ 0 & 0 & 0 & \cdots & 0 & \dfrac{\langle\sigma^{\zeta}_{zz}\rangle^{\circ}_{N-1,N}}{\langle P^{z}_{N}\rangle^{\circ}} \\ 0 & 0 & 0 & \cdots & 0 & 0 \end{bmatrix} \tag{28}$$

While the completed composite cylinder remains supported by the mandrel, the average stresses in the mandrel and layers follow by adding the above self-stress and relaxation stresses,

$$\boldsymbol{\sigma}^{\gamma}_{\theta\theta} = \boldsymbol{S}^{\gamma}_{\theta\theta}\boldsymbol{P}^{\theta} + \boldsymbol{S}^{\gamma}_{\theta z}\boldsymbol{P}^{z} \qquad \boldsymbol{\sigma}^{\gamma}_{zz} = \boldsymbol{S}^{\gamma}_{z\theta}\boldsymbol{P}^{\theta} + \boldsymbol{S}^{\gamma}_{zz}\boldsymbol{P}^{z} \tag{29}$$

where

$$\boldsymbol{\sigma}^{\gamma}_{\theta\theta} = \boldsymbol{\sigma}^{\alpha}_{\theta\theta} + \boldsymbol{\sigma}^{\beta}_{\theta\theta} \qquad \boldsymbol{\sigma}^{\gamma}_{zz} = \boldsymbol{\sigma}^{\alpha}_{zz} + \boldsymbol{\sigma}^{\beta}_{zz} \tag{30}$$

and

$$\boldsymbol{S}^{\gamma}_{\theta\theta} = \boldsymbol{S}^{\alpha}_{\theta\theta} + \boldsymbol{S}^{\beta}_{\theta\theta} \qquad \boldsymbol{S}^{\gamma}_{\theta z} = \boldsymbol{S}^{\alpha}_{\theta z} + \boldsymbol{S}^{\beta}_{\theta z} \tag{31}$$

$$\boldsymbol{S}^{\gamma}_{z\theta} = \boldsymbol{S}^{\alpha}_{z\theta} + \boldsymbol{S}^{\beta}_{z\theta} \qquad \boldsymbol{S}^{\gamma}_{zz} = \boldsymbol{S}^{\alpha}_{zz} + \boldsymbol{S}^{\beta}_{zz} \tag{32}$$

2.3. Mandrel reaction stresses

The radial and axial reactions exerted by the mandrel on the completed structure can now be evaluated from (19) and (21) as

$$R = \sum_{j=2}^{N} \left\{ \left[\frac{\langle\sigma^{\rho}_{rr}\rangle^{\circ}_{1,j}}{\langle P^{\theta}_{j}\rangle^{\circ}} \right] P^{\theta}_{j} + \left[\frac{\langle\sigma^{\zeta}_{rr}\rangle^{\circ}_{1,j}}{\langle P^{z}_{j}\rangle^{\circ}} \right] P^{z}_{j} \right\} \tag{33}$$

$$Z = \sum_{j=2}^{N} \left\{ \left[\frac{\langle\sigma^{\rho}_{zz}\rangle^{\circ}_{1,j}}{\langle P^{\theta}_{j}\rangle^{\circ}} \right] P^{\theta}_{j} + \left[\frac{\langle\sigma^{\zeta}_{zz}\rangle^{\circ}_{1,j}}{\langle P^{z}_{j}\rangle^{\circ}} \right] P^{z}_{j} \right\} \tag{34}$$

The effect of the mandrel removal is equivalent to application of the radial traction $-R$ at the inner surface $r = a_2$ and $-Z$, at both ends of the no longer mandrel supported cylindrical structure. The corresponding components of average stresses in the layers are,

$$\langle\sigma^{i}_{\theta\theta}\rangle^{R} = -R\langle\sigma^{r}_{\theta\theta}\rangle^{\circ}_{i} \qquad \langle\sigma^{i}_{\theta\theta}\rangle^{Z} = -Z\langle\sigma^{a}_{\theta\theta}\rangle^{\circ}_{i} \tag{35}$$

$$\langle\sigma^{i}_{zz}\rangle^{R} = -R\langle\sigma^{r}_{zz}\rangle^{\circ}_{i} \qquad \langle\sigma^{i}_{zz}\rangle^{Z} = -Z\langle\sigma^{a}_{zz}\rangle^{\circ}_{i} \tag{36}$$

where the $\langle\sigma^{r}_{\theta\theta}\rangle^{\circ}_{i}$ and $\langle\sigma^{r}_{zz}\rangle^{\circ}_{i}$ are layer average stresses due to unit radial pressure $-P_a/(a_2L) = 1$ applied at $r = a_2$ and $\langle\sigma^{a}_{\theta\theta}\rangle^{\circ}_{i}$ and $\langle\sigma^{a}_{zz}\rangle^{\circ}_{i}$ are the layer average stresses caused by a unit axial stress $P_z/[\pi(b_1^2 - a_1^2)] = 1$, respectively; both are dimensionless.

Using the matrix form, eqns (35) and (36) are written as

$$\boldsymbol{\sigma}^R_{\theta\theta} = \boldsymbol{S}^R_{\theta\theta}\boldsymbol{P}^\theta + \boldsymbol{S}^R_{\theta z}\boldsymbol{P}^z \quad \boldsymbol{\sigma}^Z_{\theta\theta} = \boldsymbol{S}^Z_{\theta\theta}\boldsymbol{P}^\theta + \boldsymbol{S}^Z_{\theta z}\boldsymbol{P}^z \tag{37}$$

$$\boldsymbol{\sigma}^R_{zz} = \boldsymbol{S}^R_{z\theta}\boldsymbol{P}^\theta + \boldsymbol{S}^R_{zz}\boldsymbol{P}^z \quad \boldsymbol{\sigma}^Z_{zz} = \boldsymbol{S}^Z_{z\theta}\boldsymbol{P}^\theta + \boldsymbol{S}^Z_{zz}\boldsymbol{P}^z \tag{38}$$

where the $[(N-1)\times 1]$ stress vectors are

$$\boldsymbol{\sigma}^R_{\theta\theta} = [\langle\sigma^2_{\theta\theta}\rangle^R, \langle\sigma^3_{\theta\theta}\rangle^R, \langle\sigma^4_{\theta\theta}\rangle^R, \ldots, \langle\sigma^N_{\theta\theta}\rangle^R] \tag{39}$$

$$\boldsymbol{\sigma}^Z_{\theta\theta} = [\langle\sigma^2_{\theta\theta}\rangle^Z, \langle\sigma^3_{\theta\theta}\rangle^Z, \langle\sigma^4_{\theta\theta}\rangle^Z, \ldots, \langle\sigma^N_{\theta\theta}\rangle^Z] \tag{40}$$

$$\boldsymbol{\sigma}^R_{zz} = [\langle\sigma^2_{zz}\rangle^R, \langle\sigma^3_{zz}\rangle^R, \langle\sigma^4_{zz}\rangle^R, \ldots, \langle\sigma^N_{zz}\rangle^R] \tag{41}$$

$$\boldsymbol{\sigma}^Z_{zz} = [\langle\sigma^2_{zz}\rangle^Z, \langle\sigma^3_{zz}\rangle^Z, \langle\sigma^4_{zz}\rangle^R, \ldots, \langle\sigma^N_{zz}\rangle^Z] \tag{42}$$

The $[(N-1)\times(N-1)]$ stress influence functions in (37) and (38) are

$$\boldsymbol{S}^R_{\theta\theta} = \begin{bmatrix} -\dfrac{\langle\sigma^\rho_{rr}\rangle^\circ_{1,2}\langle\sigma^r_{\theta\theta}\rangle^\circ_2}{\langle P^\theta_2\rangle^\circ} & -\dfrac{\langle\sigma^\rho_{rr}\rangle^\circ_{1,3}\langle\sigma^r_{\theta\theta}\rangle^\circ_2}{\langle P^\theta_3\rangle^\circ} & \cdots & -\dfrac{\langle\sigma^\rho_{rr}\rangle^\circ_{1,N}\langle\sigma^r_{\theta\theta}\rangle^\circ_2}{\langle P^\theta_N\rangle^\circ} \\ -\dfrac{\langle\sigma^\rho_{rr}\rangle^\circ_{1,2}\langle\sigma^r_{\theta\theta}\rangle^\circ_3}{\langle P^\theta_2\rangle^\circ} & -\dfrac{\langle\sigma^\rho_{rr}\rangle^\circ_{1,3}\langle\sigma^r_{\theta\theta}\rangle^\circ_3}{\langle P^\theta_3\rangle^\circ} & \cdots & -\dfrac{\langle\sigma^\rho_{rr}\rangle^\circ_{1,N}\langle\sigma^r_{\theta\theta}\rangle^\circ_3}{\langle P^\theta_N\rangle^\circ} \\ \vdots & \vdots & \ddots & \vdots \\ -\dfrac{\langle\sigma^\rho_{rr}\rangle^\circ_{1,2}\langle\sigma^r_{\theta\theta}\rangle^\circ_N}{\langle P^\theta_2\rangle^\circ} & -\dfrac{\langle\sigma^\rho_{rr}\rangle^\circ_{1,3}\langle\sigma^r_{\theta\theta}\rangle^\circ_N}{\langle P^\theta_3\rangle^\circ} & \cdots & -\dfrac{\langle\sigma^\rho_{rr}\rangle^\circ_{1,N}\langle\sigma^r_{\theta\theta}\rangle^\circ_N}{\langle P^\theta_N\rangle^\circ} \end{bmatrix} \tag{43}$$

$$\boldsymbol{S}^Z_{\theta\theta} = \begin{bmatrix} -\dfrac{\langle\sigma^\rho_{zz}\rangle^\circ_{1,2}\langle\sigma^a_{\theta\theta}\rangle^\circ_2}{\langle P^\theta_2\rangle^\circ} & -\dfrac{\langle\sigma^\rho_{zz}\rangle^\circ_{1,3}\langle\sigma^a_{\theta\theta}\rangle^\circ_2}{\langle P^\theta_3\rangle^\circ} & \cdots & -\dfrac{\langle\sigma^\rho_{zz}\rangle^\circ_{1,N}\langle\sigma^a_{\theta\theta}\rangle^\circ_2}{\langle P^\theta_N\rangle^\circ} \\ -\dfrac{\langle\sigma^\rho_{zz}\rangle^\circ_{1,2}\langle\sigma^a_{\theta\theta}\rangle^\circ_3}{\langle P^\theta_2\rangle^\circ} & -\dfrac{\langle\sigma^\rho_{zz}\rangle^\circ_{1,3}\langle\sigma^a_{\theta\theta}\rangle^\circ_3}{\langle P^\theta_3\rangle^\circ} & \cdots & -\dfrac{\langle\sigma^\rho_{zz}\rangle^\circ_{1,N}\langle\sigma^a_{\theta\theta}\rangle^\circ_3}{\langle P^\theta_N\rangle^\circ} \\ \vdots & \vdots & \ddots & \vdots \\ -\dfrac{\langle\sigma^\rho_{zz}\rangle^\circ_{1,2}\langle\sigma^a_{\theta\theta}\rangle^\circ_N}{\langle P^\theta_2\rangle^\circ} & -\dfrac{\langle\sigma^\rho_{zz}\rangle^\circ_{1,3}\langle\sigma^a_{\theta\theta}\rangle^\circ_N}{\langle P^\theta_3\rangle^\circ} & \cdots & -\dfrac{\langle\sigma^\rho_{zz}\rangle^\circ_{1,N}\langle\sigma^a_{\theta\theta}\rangle^\circ_N}{\langle P^\theta_N\rangle^\circ} \end{bmatrix} \tag{44}$$

$$\boldsymbol{S}^R_{\theta z} = \begin{bmatrix} -\dfrac{\langle\sigma^\zeta_{rr}\rangle^\circ_{1,2}\langle\sigma^r_{\theta\theta}\rangle^\circ_2}{\langle P^z_2\rangle^\circ} & -\dfrac{\langle\sigma^\zeta_{rr}\rangle^\circ_{1,3}\langle\sigma^r_{\theta\theta}\rangle^\circ_2}{\langle P^z_3\rangle^\circ} & \cdots & -\dfrac{\langle\sigma^\zeta_{rr}\rangle^\circ_{1,N}\langle\sigma^r_{\theta\theta}\rangle^\circ_2}{\langle P^z_N\rangle^\circ} \\ -\dfrac{\langle\sigma^\zeta_{rr}\rangle^\circ_{1,2}\langle\sigma^r_{\theta\theta}\rangle^\circ_3}{\langle P^z_2\rangle^\circ} & -\dfrac{\langle\sigma^\zeta_{rr}\rangle^\circ_{1,3}\langle\sigma^r_{\theta\theta}\rangle^\circ_3}{\langle P^z_3\rangle^\circ} & \cdots & -\dfrac{\langle\sigma^\zeta_{rr}\rangle^\circ_{1,N}\langle\sigma^r_{\theta\theta}\rangle^\circ_3}{\langle P^z_N\rangle^\circ} \\ \vdots & \vdots & \ddots & \vdots \\ -\dfrac{\langle\sigma^\zeta_{rr}\rangle^\circ_{1,2}\langle\sigma^r_{\theta\theta}\rangle^\circ_N}{\langle P^z_2\rangle^\circ} & -\dfrac{\langle\sigma^\zeta_{rr}\rangle^\circ_{1,3}\langle\sigma^r_{\theta\theta}\rangle^\circ_N}{\langle P^z_3\rangle^\circ} & \cdots & -\dfrac{\langle\sigma^\zeta_{rr}\rangle^\circ_{1,N}\langle\sigma^r_{\theta\theta}\rangle^\circ_N}{\langle P^z_N\rangle^\circ} \end{bmatrix} \tag{45}$$

$$\boldsymbol{S}^{Z}_{\theta z} = \begin{bmatrix} -\dfrac{\langle\sigma^{\zeta}_{zz}\rangle^{\circ}_{1,2}\langle\sigma^{a}_{\theta\theta}\rangle^{\circ}_{2}}{\langle P^{z}_{2}\rangle^{\circ}} & -\dfrac{\langle\sigma^{\zeta}_{zz}\rangle^{\circ}_{1,3}\langle\sigma^{a}_{\theta\theta}\rangle^{\circ}_{2}}{\langle P^{z}_{3}\rangle^{\circ}} & \cdots & -\dfrac{\langle\sigma^{\zeta}_{zz}\rangle^{\circ}_{1,N}\langle\sigma^{a}_{\theta\theta}\rangle^{\circ}_{2}}{\langle P^{z}_{N}\rangle^{\circ}} \\ -\dfrac{\langle\sigma^{\zeta}_{zz}\rangle^{\circ}_{1,2}\langle\sigma^{a}_{\theta\theta}\rangle^{\circ}_{3}}{\langle P^{z}_{2}\rangle^{\circ}} & -\dfrac{\langle\sigma^{\zeta}_{zz}\rangle^{\circ}_{1,3}\langle\sigma^{a}_{\theta\theta}\rangle^{\circ}_{3}}{\langle P^{z}_{3}\rangle^{\circ}} & \cdots & -\dfrac{\langle\sigma^{\zeta}_{zz}\rangle^{\circ}_{1,N}\langle\sigma^{a}_{\theta\theta}\rangle^{\circ}_{3}}{\langle P^{z}_{N}\rangle^{\circ}} \\ \vdots & \vdots & \ddots & \vdots \\ -\dfrac{\langle\sigma^{\zeta}_{zz}\rangle^{\circ}_{1,2}\langle\sigma^{a}_{\theta\theta}\rangle^{\circ}_{N}}{\langle P^{z}_{2}\rangle^{\circ}} & -\dfrac{\langle\sigma^{\zeta}_{zz}\rangle^{\circ}_{1,3}\langle\sigma^{a}_{\theta\theta}\rangle^{\circ}_{N}}{\langle P^{z}_{3}\rangle^{\circ}} & \cdots & -\dfrac{\langle\sigma^{\zeta}_{zz}\rangle^{\circ}_{1,N}\langle\sigma^{a}_{\theta\theta}\rangle^{\circ}_{N}}{\langle P^{z}_{N}\rangle^{\circ}} \end{bmatrix} \tag{46}$$

$$\boldsymbol{S}^{R}_{z\theta} = \begin{bmatrix} -\dfrac{\langle\sigma^{\rho}_{rr}\rangle^{\circ}_{1,2}\langle\sigma^{r}_{zz}\rangle^{\circ}_{2}}{\langle P^{\theta}_{2}\rangle^{\circ}} & -\dfrac{\langle\sigma^{\rho}_{rr}\rangle^{\circ}_{1,3}\langle\sigma^{r}_{zz}\rangle^{\circ}_{2}}{\langle P^{\theta}_{3}\rangle^{\circ}} & \cdots & -\dfrac{\langle\sigma^{\rho}_{rr}\rangle^{\circ}_{1,N}\langle\sigma^{r}_{zz}\rangle^{\circ}_{2}}{\langle P^{\theta}_{N}\rangle^{\circ}} \\ -\dfrac{\langle\sigma^{\rho}_{rr}\rangle^{\circ}_{1,2}\langle\sigma^{r}_{zz}\rangle^{\circ}_{3}}{\langle P^{\theta}_{2}\rangle^{\circ}} & -\dfrac{\langle\sigma^{\rho}_{rr}\rangle^{\circ}_{1,3}\langle\sigma^{r}_{zz}\rangle^{\circ}_{3}}{\langle P^{\theta}_{3}\rangle^{\circ}} & \cdots & -\dfrac{\langle\sigma^{\rho}_{rr}\rangle^{\circ}_{1,N}\langle\sigma^{r}_{zz}\rangle^{\circ}_{3}}{\langle P^{\theta}_{N}\rangle^{\circ}} \\ \vdots & \vdots & \ddots & \vdots \\ -\dfrac{\langle\sigma^{\rho}_{rr}\rangle^{\circ}_{1,2}\langle\sigma^{r}_{zz}\rangle^{\circ}_{N}}{\langle P^{\theta}_{2}\rangle^{\circ}} & -\dfrac{\langle\sigma^{\rho}_{rr}\rangle^{\circ}_{1,3}\langle\sigma^{r}_{zz}\rangle^{\circ}_{N}}{\langle P^{\theta}_{3}\rangle^{\circ}} & \cdots & -\dfrac{\langle\sigma^{\rho}_{rr}\rangle^{\circ}_{1,N}\langle\sigma^{r}_{zz}\rangle^{\circ}_{N}}{\langle P^{\theta}_{N}\rangle^{\circ}} \end{bmatrix} \tag{47}$$

$$\boldsymbol{S}^{Z}_{z\theta} = \begin{bmatrix} -\dfrac{\langle\sigma^{\rho}_{zz}\rangle^{\circ}_{1,2}\langle\sigma^{a}_{zz}\rangle^{\circ}_{2}}{\langle P^{\theta}_{2}\rangle^{\circ}} & -\dfrac{\langle\sigma^{\rho}_{zz}\rangle^{\circ}_{1,3}\langle\sigma^{a}_{zz}\rangle^{\circ}_{2}}{\langle P^{\theta}_{3}\rangle^{\circ}} & \cdots & -\dfrac{\langle\sigma^{\rho}_{zz}\rangle^{\circ}_{1,N}\langle\sigma^{a}_{zz}\rangle^{\circ}_{2}}{\langle P^{\theta}_{N}\rangle^{\circ}} \\ -\dfrac{\langle\sigma^{\rho}_{zz}\rangle^{\circ}_{1,2}\langle\sigma^{a}_{zz}\rangle^{\circ}_{3}}{\langle P^{\theta}_{2}\rangle^{\circ}} & -\dfrac{\langle\sigma^{\rho}_{zz}\rangle^{\circ}_{1,3}\langle\sigma^{a}_{zz}\rangle^{\circ}_{3}}{\langle P^{\theta}_{3}\rangle^{\circ}} & \cdots & -\dfrac{\langle\sigma^{\rho}_{zz}\rangle^{\circ}_{1,N}\langle\sigma^{a}_{zz}\rangle^{\circ}_{3}}{\langle P^{\theta}_{N}\rangle^{\circ}} \\ \vdots & \vdots & \ddots & \vdots \\ -\dfrac{\langle\sigma^{\rho}_{zz}\rangle^{\circ}_{1,2}\langle\sigma^{a}_{zz}\rangle^{\circ}_{N}}{\langle P^{\theta}_{2}\rangle^{\circ}} & -\dfrac{\langle\sigma^{\rho}_{zz}\rangle^{\circ}_{1,3}\langle\sigma^{a}_{zz}\rangle^{\circ}_{N}}{\langle P^{\theta}_{3}\rangle^{\circ}} & \cdots & -\dfrac{\langle\sigma^{\rho}_{zz}\rangle^{\circ}_{1,N}\langle\sigma^{a}_{zz}\rangle^{\circ}_{N}}{\langle P^{\theta}_{N}\rangle^{\circ}} \end{bmatrix} \tag{48}$$

$$\boldsymbol{S}^{R}_{zz} = \begin{bmatrix} -\dfrac{\langle\sigma^{\zeta}_{rr}\rangle^{\circ}_{1,2}\langle\sigma^{r}_{zz}\rangle^{\circ}_{2}}{\langle P^{z}_{2}\rangle^{\circ}} & -\dfrac{\langle\sigma^{\zeta}_{rr}\rangle^{\circ}_{1,3}\langle\sigma^{r}_{zz}\rangle^{\circ}_{2}}{\langle P^{z}_{3}\rangle^{\circ}} & \cdots & -\dfrac{\langle\sigma^{\zeta}_{rr}\rangle^{\circ}_{1,N}\langle\sigma^{r}_{zz}\rangle^{\circ}_{2}}{\langle P^{z}_{N}\rangle^{\circ}} \\ -\dfrac{\langle\sigma^{\zeta}_{rr}\rangle^{\circ}_{1,2}\langle\sigma^{r}_{zz}\rangle^{\circ}_{3}}{\langle P^{z}_{2}\rangle^{\circ}} & -\dfrac{\langle\sigma^{\zeta}_{rr}\rangle^{\circ}_{1,3}\langle\sigma^{r}_{zz}\rangle^{\circ}_{3}}{\langle P^{z}_{3}\rangle^{\circ}} & \cdots & -\dfrac{\langle\sigma^{\zeta}_{rr}\rangle^{\circ}_{1,N}\langle\sigma^{r}_{zz}\rangle^{\circ}_{3}}{\langle P^{z}_{N}\rangle^{\circ}} \\ \vdots & \vdots & \ddots & \vdots \\ -\dfrac{\langle\sigma^{\zeta}_{rr}\rangle^{\circ}_{1,2}\langle\sigma^{r}_{zz}\rangle^{\circ}_{N}}{\langle P^{z}_{2}\rangle^{\circ}} & -\dfrac{\langle\sigma^{\zeta}_{rr}\rangle^{\circ}_{1,3}\langle\sigma^{r}_{zz}\rangle^{\circ}_{N}}{\langle P^{z}_{3}\rangle^{\circ}} & \cdots & -\dfrac{\langle\sigma^{\zeta}_{rr}\rangle^{\circ}_{1,N}\langle\sigma^{r}_{zz}\rangle^{\circ}_{N}}{\langle P^{z}_{N}\rangle^{\circ}} \end{bmatrix} \tag{49}$$

$$\boldsymbol{S}_{zz}^{Z} = \begin{bmatrix} -\dfrac{\langle\sigma_{zz}^{\zeta}\rangle_{1,2}^{\circ}\langle\sigma_{zz}^{a}\rangle_{2}^{\circ}}{\langle P_2^z\rangle^{\circ}} & -\dfrac{\langle\sigma_{zz}^{\zeta}\rangle_{1,3}^{\circ}\langle\sigma_{zz}^{a}\rangle_{2}^{\circ}}{\langle P_3^z\rangle^{\circ}} & \cdots & -\dfrac{\langle\sigma_{zz}^{\zeta}\rangle_{1,N}^{\circ}\langle\sigma_{zz}^{a}\rangle_{2}^{\circ}}{\langle P_N^z\rangle^{\circ}} \\ -\dfrac{\langle\sigma_{zz}^{\zeta}\rangle_{1,2}^{\circ}\langle\sigma_{zz}^{a}\rangle_{3}^{\circ}}{\langle P_2^z\rangle^{\circ}} & -\dfrac{\langle\sigma_{zz}^{\zeta}\rangle_{1,3}^{\circ}\langle\sigma_{zz}^{a}\rangle_{3}^{\circ}}{\langle P_3^z\rangle^{\circ}} & \cdots & -\dfrac{\langle\sigma_{zz}^{\zeta}\rangle_{1,N}^{\circ}\langle\sigma_{zz}^{a}\rangle_{3}^{\circ}}{\langle P_N^z\rangle^{\circ}} \\ \vdots & \vdots & \ddots & \vdots \\ -\dfrac{\langle\sigma_{zz}^{\zeta}\rangle_{1,2}^{\circ}\langle\sigma_{zz}^{a}\rangle_{N}^{\circ}}{\langle P_2^z\rangle^{\circ}} & -\dfrac{\langle\sigma_{zz}^{\zeta}\rangle_{1,3}^{\circ}\langle\sigma_{zz}^{a}\rangle_{N}^{\circ}}{\langle P_3^z\rangle^{\circ}} & \cdots & -\dfrac{\langle\sigma_{zz}^{\zeta}\rangle_{1,N}^{\circ}\langle\sigma_{zz}^{a}\rangle_{N}^{\circ}}{\langle P_N^z\rangle^{\circ}} \end{bmatrix} \tag{50}$$

The total average stresses in the layers caused by application of tractions $-R$ and $-Z$ in (35) and (36) are then equal to

$$\boldsymbol{\sigma}_{\theta\theta}^{\delta} = \boldsymbol{S}_{\theta\theta}^{\delta}\boldsymbol{P}^{\theta} + \boldsymbol{S}_{\theta z}^{\delta}\boldsymbol{P}^{z} \qquad \boldsymbol{\sigma}_{zz}^{\delta} = \boldsymbol{S}_{z\theta}^{\delta}\boldsymbol{P}^{\theta} + \boldsymbol{S}_{zz}^{\delta}\boldsymbol{P}^{z} \tag{51}$$

where

$$\boldsymbol{S}_{\theta\theta}^{\delta} = \boldsymbol{S}_{\theta\theta}^{R} + \boldsymbol{S}_{\theta\theta}^{Z} \qquad \boldsymbol{S}_{\theta z}^{\delta} = \boldsymbol{S}_{\theta z}^{R} + \boldsymbol{S}_{\theta z}^{Z} \tag{52}$$

$$\boldsymbol{S}_{z\theta}^{\delta} = \boldsymbol{S}_{z\theta}^{R} + \boldsymbol{S}_{z\theta}^{Z} \qquad \boldsymbol{S}_{zz}^{\delta} = \boldsymbol{S}_{zz}^{R} + \boldsymbol{S}_{zz}^{Z} \tag{53}$$

2.4. Total residual stresses

A superposition of the layer stress averages due to self-stress, relaxation stress and reaction stresses provides the total residual stress state in all layers of the composite structure. Thus, adding equations $(10)_1$, $(24)_1$ and $(51)_1$ yields the overall residual hoop stress while equation $(10)_2$, $(24)_2$ and $(51)_2$ give the overall residual axial stress. These stresses can then be written as,

$$\boldsymbol{\sigma}_{\theta\theta} = \boldsymbol{S}_{\theta\theta}\boldsymbol{P}^{\theta} + \boldsymbol{S}_{\theta z}\boldsymbol{P}^{z} \qquad \boldsymbol{\sigma}_{zz} = \boldsymbol{S}_{z\theta}\boldsymbol{P}^{\theta} + \boldsymbol{S}_{zz}\boldsymbol{P}^{z} \tag{54}$$

where again, the influence functions have the dimensions $[(N-1)\times(N-1)]$ and are given by

$$\boldsymbol{S}_{\theta\theta} = \boldsymbol{S}_{\theta\theta}^{\alpha} + \boldsymbol{S}_{\theta\theta}^{\beta} + \boldsymbol{S}_{\theta\theta}^{\delta} \qquad \boldsymbol{S}_{\theta z} = \boldsymbol{S}_{\theta z}^{\alpha} + \boldsymbol{S}_{\theta z}^{\beta} + \boldsymbol{S}_{\theta z}^{\delta} \tag{55}$$

$$\boldsymbol{S}_{z\theta} = \boldsymbol{S}_{z\theta}^{\alpha} + \boldsymbol{S}_{z\theta}^{\beta} + \boldsymbol{S}_{z\theta}^{\delta} \qquad \boldsymbol{S}_{zz} = \boldsymbol{S}_{zz}^{\alpha} + \boldsymbol{S}_{zz}^{\beta} + \boldsymbol{S}_{zz}^{\delta} \tag{56}$$

2.5. Equilibrium constraints

Here we introduce force equilibrium equations that impose certain constraints on the two residual fields (29) and (54) and on the reaction stresses (51). First, consider the stress state in the completed structure still supported by the mandrel. In the absence of any external loads, Fig. 2, the force equilibrium in the hoop and axial directions, for the stresses (29), becomes

$$L[(b_1-a_1)\langle\sigma_{\theta\theta}^{1}\rangle^{\gamma} + (b_2-a_2)\langle\sigma_{\theta\theta}^{2}\rangle^{\gamma} + (b_3-a_3)\langle\sigma_{\theta\theta}^{3}\rangle^{\gamma} + \cdots + (b_N-a_N)\langle\sigma_{\theta\theta}^{N}\rangle^{\gamma}] = 0 \tag{57}$$

$$\pi[(b_1^2-a_1^2)\langle\sigma_{zz}^{1}\rangle^{\gamma} + (b_2^2-a_2^2)\langle\sigma_{zz}^{2}\rangle^{\gamma} + (b_3^2-a_3^2)\langle\sigma_{zz}^{3}\rangle^{\gamma} + \cdots + (b_N^2-a_N^2)\langle\sigma_{zz}^{N}\rangle^{\gamma}] = 0 \tag{58}$$

The stress components $\langle\sigma_{\theta\theta}^{i}\rangle^{\gamma}$ and $\langle\sigma_{zz}^{i}\rangle^{\gamma}$ can be expressed in the matrix form

$$\langle\sigma_{\theta\theta}^{i}\rangle^{\gamma} = [\boldsymbol{S}_{\theta\theta}^{(i-1)}]^{\gamma}\boldsymbol{P}^{\theta} + [\boldsymbol{S}_{\theta z}^{(i-1)}]^{\gamma}\boldsymbol{P}^{z} \quad i = 2,3,4,\ldots,N \tag{59}$$

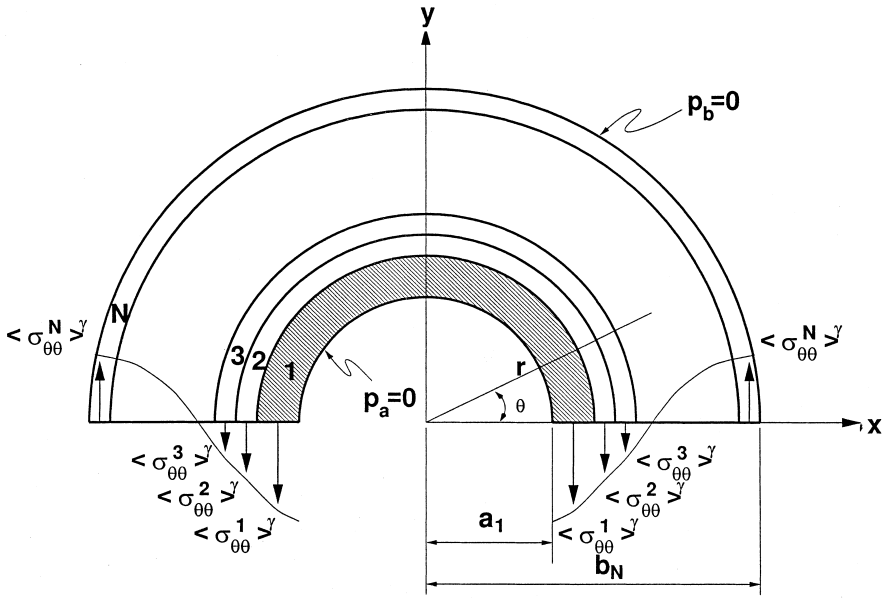

Fig. 2. Equilibrium stress state in the mandrel-supported cylinder.

$$\langle\sigma_{zz}\rangle_i^\gamma = [\boldsymbol{S}_{z\theta}^{(i-1)}]^\gamma \boldsymbol{P}^\theta + [\boldsymbol{S}_{zz}^{(i-1)}]^\gamma \boldsymbol{P}^z \qquad i = 2,3,4,\ldots,N \tag{60}$$

where $[\boldsymbol{S}^j_{\theta\theta}]^\gamma$, $[\boldsymbol{S}^j_{\theta z}]^\gamma$, $[\boldsymbol{S}^j_{z\theta}]^\gamma$ and $[\boldsymbol{S}^j_{zz}]^\gamma$ are the $[1\times(N-1)]$ row vectors formed out of the jth row of the influence functions $\boldsymbol{S}^\gamma_{\theta\theta}$, $\boldsymbol{S}^\gamma_{\theta z}$, $\boldsymbol{S}^\gamma_{z\theta}$ and $\boldsymbol{S}^\gamma_{zz}$ in (31) and (32), respectively.

Substituting the stress relations (59) and (60) in the force equilibrium conditions (57) and (58) gives,

$$(b_1-a_1)\langle\sigma^1_{\theta\theta}\rangle^\gamma + \sum_{i=2}^{N}(b_i-a_i)\{[\boldsymbol{S}_{\theta\theta}^{(i-1)}]^\gamma \boldsymbol{P}^\theta + [\boldsymbol{S}_{\theta z}^{(i-1)}]^\gamma \boldsymbol{P}^z\} = 0 \tag{61}$$

$$(b_1^2-a_1^2)\langle\sigma^1_{zz}\rangle^\gamma + \sum_{i=2}^{N}(b_i^2-a_i^2)\{[\boldsymbol{S}_{z\theta}^{(i-1)}]^\gamma \boldsymbol{P}^\theta + [\boldsymbol{S}_{zz}^{(i-1)}]^\gamma \boldsymbol{P}^z\} = 0 \tag{62}$$

Next, consider the stress state (51) caused in the completed and unsupported structure, assumed now to be free of residual stress, by the traction $-R$ applied at the inner surface $r = a_2$ as shown in Fig. 3. Force equilibrium in the hoop and axial directions provides:

$$L[(b_2-a_2)\langle\sigma^2_{\theta\theta}\rangle^R + (b_3-a_3)\langle\sigma^3_{\theta\theta}\rangle^R + (b_4-a_4)\langle\sigma^4_{\theta\theta}\rangle^R + \cdots + (b_N-a_N)\langle\sigma^N_{\theta\theta}\rangle^R] = Ra_2L \tag{63}$$

$$\pi[(b_2^2-a_2^2)\langle\sigma^2_{zz}\rangle^R + (b_3^2-a_3^2)\langle\sigma^3_{zz}\rangle^R + (b_4^2-a_4^2)\langle\sigma^4_{zz}\rangle^R + \cdots + (b_N^2-a_N^2)\langle\sigma^N_{zz}\rangle^R] = 0 \tag{64}$$

Substituting for the stress components in the above equations from $(37)_1$ and $(38)_1$,

$$-Ra_2 + \sum_{i=2}^{N}(b_i-a_i)\{[\boldsymbol{S}_{\theta\theta}^{(i-1)}]^R \boldsymbol{P}^\theta + [\boldsymbol{S}_{\theta z}^{(i-1)}]^R \boldsymbol{P}^z\} = 0 \tag{65}$$

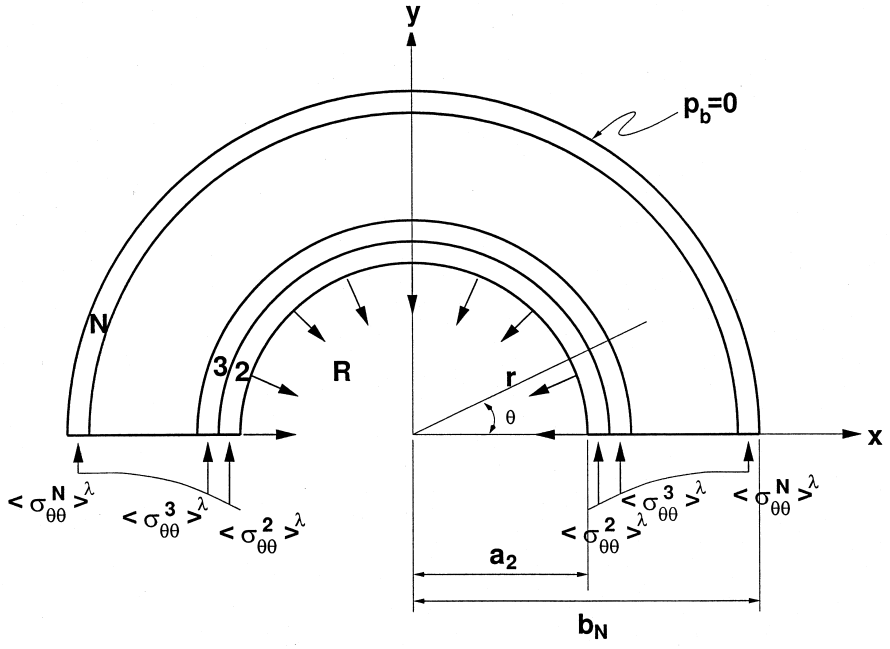

Fig. 3. Equilibrium stress state in the cylinder after mandrel removal.

$$\sum_{i=2}^{N}(b_i^2-a_i^2)\{[\boldsymbol{S}_{z\theta}^{(i-1)}]^R\boldsymbol{P}^\theta+[\boldsymbol{S}_{zz}^{(i-1)}]^R\boldsymbol{P}^z\}=0 \tag{66}$$

where $[\boldsymbol{S}^j_{\theta\theta}]^R$, $[\boldsymbol{S}^j_{\theta z}]^R$, $[\boldsymbol{S}^j_{z\theta}]^R$ and $[\boldsymbol{S}^j_{zz}]^R$ are $[1\times(N-1)]$ row vectors formed out of the jth row of the influence functions $\boldsymbol{S}^R_{\theta\theta}$, $\boldsymbol{S}^R_{\theta z}$, $\boldsymbol{S}^R_{z\theta}$ and $\boldsymbol{S}^R_{zz}$, respectively.

Similarly, if the axial forces $-Z$ are applied to both ends of the stress-free and unsupported composite structure, the force equilibrium for the fields $(37)_2$ and $(38)_2$ can be written as,

$$\sum_{i=2}^{N}(b_i-a_i)\{[\boldsymbol{S}_{\theta\theta}^{(i-1)}]^Z\boldsymbol{P}^\theta+[\boldsymbol{S}_{\theta z}^{(i-1)}]^Z\boldsymbol{P}^z\}=0 \tag{67}$$

$$-Z(b_1^2-a_1^2)+\sum_{i=2}^{N}(b_i^2-a_i^2)\{[\boldsymbol{S}_{z\theta}^{(i-1)}]^Z\boldsymbol{P}^\theta+[\boldsymbol{S}_{zz}^{(i-1)}]^Z\boldsymbol{P}^z\}=0 \tag{68}$$

where $[\boldsymbol{S}^j_{\theta\theta}]^Z$, $[\boldsymbol{S}^j_{\theta z}]^Z$, $[\boldsymbol{S}^j_{z\theta}]^Z$ and $[\boldsymbol{S}^j_{zz}]^Z$ are $[1\times(N-1)]$ row vectors formed out of the jth row of the influence functions $\boldsymbol{S}^Z_{\theta\theta}$, $\boldsymbol{S}^Z_{\theta z}$, $\boldsymbol{S}^Z_{z\theta}$ and $\boldsymbol{S}^Z_{zz}$, respectively.

Now, adding the hoop stress relations (61), (65) and (67) and the axial stress relations (62), (66) and (68) gives,

$$-a_2R+(b_1-a_1)\langle\sigma^1_{\theta\theta}\rangle^\gamma+\sum_{i=2}^{N}(b_i-a_i)\{([\boldsymbol{S}_{\theta\theta}^{(i-1)}]^\gamma+[\boldsymbol{S}_{\theta\theta}^{(i-1)}]^R+[\boldsymbol{S}_{\theta\theta}^{(i-1)}]^Z)\boldsymbol{P}^\theta$$
$$+([\boldsymbol{S}_{\theta z}^{(i-1)}]^\gamma+[\boldsymbol{S}_{\theta z}^{(i-1)}]^R+[\boldsymbol{S}_{\theta z}^{(i-1)}]^Z)\boldsymbol{P}^z\}=0 \tag{69}$$

$$-(b_1^2-a_1^2)Z+(b_1^2-a_1^2)\langle\sigma_{zz}^1\rangle^{\gamma}+\sum_{i=2}^{N}(b_i^2-a_i^2)\{([\boldsymbol{S}_{z\theta}^{(i-1)}]^{\gamma}+[\boldsymbol{S}_{z\theta}^{(i-1)}]^{R}+[\boldsymbol{S}_{z\theta}^{(i-1)}]^{Z})\boldsymbol{P}^{\theta}$$

$$+([\boldsymbol{S}_{zz}^{(i-1)}]^{\gamma}+[\boldsymbol{S}_{zz}^{(i-1)}]^{R}+[\boldsymbol{S}_{zz}^{(i-1)}]^{Z})\boldsymbol{P}^{z}\}=0 \quad (70)$$

Making use of (29)–(32), (37)–(38) and (51)–(56), eqns (69) and (70) can be simplified as,

$$-Ra_2+(b_1-a_1)\langle\sigma_{\theta\theta}^1\rangle^{\gamma}+\sum_{i=2}^{N}(b_i-a_i)\{\boldsymbol{S}_{\theta\theta}^{(i-1)}\boldsymbol{P}^{\theta}+\boldsymbol{S}_{\theta z}^{(i-1)}\boldsymbol{P}^{z}\}=0 \quad (71)$$

$$-(b_1^2-a_1^2)Z+(b_1^2-a_1^2)\langle\sigma_{zz}^1\rangle^{\gamma}+\sum_{i=2}^{N}(b_i^2-a_i^2)\{\boldsymbol{S}_{z\theta}^{(i-1)}\boldsymbol{P}^{\theta}+\boldsymbol{S}_{zz}^{(i-1)}\boldsymbol{P}^{z}\}=0 \quad (72)$$

where $\boldsymbol{S}_{\theta\theta}^{j}$, $\boldsymbol{S}_{\theta z}^{j}$, $\boldsymbol{S}_{z\theta}^{j}$ and $\boldsymbol{S}_{zz}^{j}$ are $[1\times(N-1)]$ row vectors formed out of the jth row of the influence functions $\boldsymbol{S}_{\theta\theta}$, $\boldsymbol{S}_{\theta z}$, $\boldsymbol{S}_{z\theta}$ and $\boldsymbol{S}_{zz}$, respectively.

Following eqns (20) and (21), the stresses $\langle\sigma_{\theta\theta}^1\rangle^{\gamma}$ and $\langle\sigma_{zz}^1\rangle^{\gamma}$ in the above equations can be expanded as,

$$\langle\sigma_{\theta\theta}^1\rangle^{\gamma}=\sum_{j=2}^{N}\left\{\left[\frac{\langle\sigma_{\theta\theta}^{\rho}\rangle_{1,j}^{\circ}}{\langle P_j^{\theta}\rangle^{\circ}}\right]P_j^{\theta}+\left[\frac{\langle\sigma_{\theta\theta}^{\zeta}\rangle_{1,j}^{\circ}}{\langle P_j^{\theta}\rangle^{\circ}}\right]P_j^{z}\right\} \quad (73)$$

$$\langle\sigma_{zz}^1\rangle^{\gamma}=\sum_{j=2}^{N}\left\{\left[\frac{\langle\sigma_{zz}^{\rho}\rangle_{1,j}^{\circ}}{\langle P_j^{\theta}\rangle^{\circ}}\right]P_j^{\theta}+\left[\frac{\langle\sigma_{zz}^{\zeta}\rangle_{1,j}^{\circ}}{\langle P_j^{\theta}\rangle^{\circ}}\right]P_j^{z}\right\} \quad (74)$$

The hoop stresses $\langle\sigma_{\theta\theta}^{\rho}\rangle_{1,j}^{\circ}$ and $\langle\sigma_{\theta\theta}^{\zeta}\rangle_{1,j}^{\circ}$ in (73) are further replaced by their corresponding radial stresses. Referring back to the construction stage (17) and (18), where the jth layer is being laid on already cured $(j-1)$ layers, a free body diagram of the mandrel along with the forces acting on it due to a unit load $\rho_j^{\circ}=1$ in the jth layer is considered, as shown in Fig. 4. The equilibrium of forces in the mandrel layer requires

$$\langle\sigma_{\theta\theta}^{\rho}\rangle_{1,j}=\frac{a_2}{(b_1-a_1)}\langle\sigma_{rr}^{\rho}\rangle_{1,j} \quad (75)$$

Similarly, the equilibrium in the mandrel due to a unit pre-stressing force $\zeta_j^{\circ}=1$ in the jth layer gives

$$\langle\sigma_{\theta\theta}^{\zeta}\rangle_{1,j}=\frac{a_2}{(b_1-a_1)}\langle\sigma_{rr}^{\zeta}\rangle_{1,j} \quad (76)$$

Substituting (75) and (76) in (73) yields:

$$\langle\sigma_{\theta\theta}^1\rangle^{\gamma}=\frac{a_2}{(b_1-a_1)}\left[\sum_{j=2}^{N}\left\{\left[\frac{\langle\sigma_{rr}^{\rho}\rangle_{1,j}^{\circ}}{\langle P_j^{\theta}\rangle^{\circ}}\right]P_j^{\theta}+\left[\frac{\langle\sigma_{rr}^{\zeta}\rangle_{1,j}^{\circ}}{\langle P_j^{z}\rangle^{\circ}}\right]P_j^{z}\right\}\right] \quad (77)$$

Comparing eqns (77) and (33), one can conclude that

$$-a_2R+(b_1-a_1)\langle\sigma_{\theta\theta}^1\rangle^{\gamma}=0 \quad (78)$$

Also, from eqns (74) and (34),

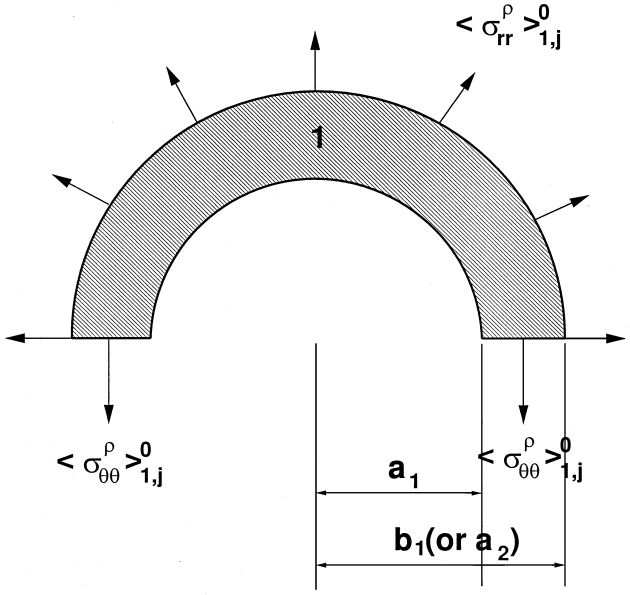

Fig. 4. Stress state in the mandrel.

$$-(b_1^2-a_1^2)Z+(b_1^2-a_1^2)\langle\sigma_{zz}^1\rangle^{\gamma}=0 \tag{79}$$

The relations (78) and (79) further simplify the eqns (71) and (72) as,

$$\sum_{i=2}^{N}(b_i-a_i)\{\boldsymbol{S}_{\theta\theta}^{(i-1)}\boldsymbol{P}^{\theta}+\boldsymbol{S}_{\theta z}^{(i-1)}\boldsymbol{P}^{z}\}=0 \tag{80}$$

$$\sum_{i=2}^{N}(b_i^2-a_i^2)\{\boldsymbol{S}_{z\theta}^{(i-1)}\boldsymbol{P}^{\theta}+\boldsymbol{S}_{zz}^{(i-1)}\boldsymbol{P}^{z}\}=0 \tag{81}$$

It is however, necessary in fabrication to apply the pre-stressing force P_i in the direction of winding. Thus, if the layer has a winding helix angle ψ_i with the cylinder axis, the hoop and axial pre-stressing forces P_i^{θ} and P_i^{z} are given by eqn (1). The pre-stressing force vectors (11) can then be written as,

$$\boldsymbol{P}^{\theta}=\boldsymbol{T}_1\boldsymbol{P}\qquad \boldsymbol{P}^{z}=\boldsymbol{T}_2\boldsymbol{P} \tag{82}$$

where $\boldsymbol{P}=[P_2,P_3,P_4,\ldots,P_N]^T$ is the resultant pre-stressing force vector of dimension $[(N-1)\times 1]$ and $\boldsymbol{T}_1$ and $\boldsymbol{T}_2$ are the transformation matrices of dimension $[(N-1)\times(N-1)]$ represented by,

$$\boldsymbol{T}_1=\begin{bmatrix}\sin\psi_2 & 0 & 0 & \ldots & 0\\ 0 & \sin\psi_3 & 0 & \ldots & 0\\ 0 & 0 & \sin\psi_4 & \ldots & 0\\ \vdots & \vdots & \vdots & \ddots & \vdots\\ 0 & 0 & 0 & \ldots & \sin\psi_N\end{bmatrix} \tag{83}$$

$$\boldsymbol{T}_2 = \begin{bmatrix} \cos\psi_2 & 0 & 0 & \dots & 0 \\ 0 & \cos\psi_3 & 0 & \dots & 0 \\ 0 & 0 & \cos\psi_4 & \dots & 0 \\ \vdots & \vdots & \vdots & \ddots & \vdots \\ 0 & 0 & 0 & \dots & \cos\psi_N \end{bmatrix} \tag{84}$$

Finally, substituting eqns (82) in (80) and (81), we get,

$$\sum_{i=2}^{N} (b_i - a_i)[\boldsymbol{S}_{\theta\theta}^{(i-1)}\boldsymbol{T}_1 + \boldsymbol{S}_{\theta z}^{(i-1)}\boldsymbol{T}_2]\boldsymbol{P} = 0 \tag{85}$$

$$\sum_{i=2}^{N} (b_i^2 - a_i^2)[\boldsymbol{S}_{z\theta}^{(i-1)}\boldsymbol{T}_1 + \boldsymbol{S}_{zz}^{(i-1)}\boldsymbol{T}_2]\boldsymbol{P} = 0 \tag{86}$$

The pre-stressing force vector can be chosen at wish. Therefore, eqns (85) and (86) lead to the following vector relations

$$\sum_{i=2}^{N} (b_i - a_i)[\boldsymbol{S}_{\theta\theta}^{(i-1)}\boldsymbol{T}_1 + \boldsymbol{S}_{\theta z}^{(i-1)}\boldsymbol{T}_2] = \boldsymbol{0} \tag{87}$$

$$\sum_{i=2}^{N} (b_i^2 - a_i^2)[\boldsymbol{S}_{z\theta}^{(i-1)}\boldsymbol{T}_1 + \boldsymbol{S}_{zz}^{(i-1)}\boldsymbol{T}_2] = \boldsymbol{0} \tag{88}$$

These imply that the row vectors formed out of the matrices $(\boldsymbol{S}_{z\theta}\boldsymbol{T}_1 + \boldsymbol{S}_{zz}\boldsymbol{T}_2)$ and $(\boldsymbol{S}_{z\theta}\boldsymbol{T}_1 + \boldsymbol{S}_{zz}\boldsymbol{T}_2)$ are linearly dependent, or in other words, these two matrices are singular with one rank deficiency.

The singular nature of each influence matrix can be determined by applying specific pre-stressing loading cases. First, let the pre-stressing forces applied be just the hoop forces P_i^{θ} in all the layers. This provides eqns (80) and (81) in the form,

$$\sum_{i=2}^{N} (b_i - a_i)\boldsymbol{S}_{\theta\theta}^{(i-1)}\boldsymbol{P}^{\theta} = 0 \tag{89}$$

$$\sum_{i=2}^{N} (b_i^2 - a_i^2)\boldsymbol{S}_{z\theta}^{(i-1)}\boldsymbol{P}^{\theta} = 0 \tag{90}$$

Again, based on the fact that the pre-stressing forces P_i^{θ} can have any magnitude, it can be concluded from the above equations that

$$\sum_{i=2}^{N} (b_i - a_i)\boldsymbol{S}_{\theta\theta}^{(i-1)} = \boldsymbol{0} \tag{91}$$

$$\sum_{i=2}^{N} (b_i^2 - a_i^2)\boldsymbol{S}_{z\theta}^{(i-1)} = \boldsymbol{0} \tag{92}$$

These relations indicate that the matrices $\boldsymbol{S}_{\theta\theta}$ and $\boldsymbol{S}_{z\theta}$ are each singular with one rank deficiency.

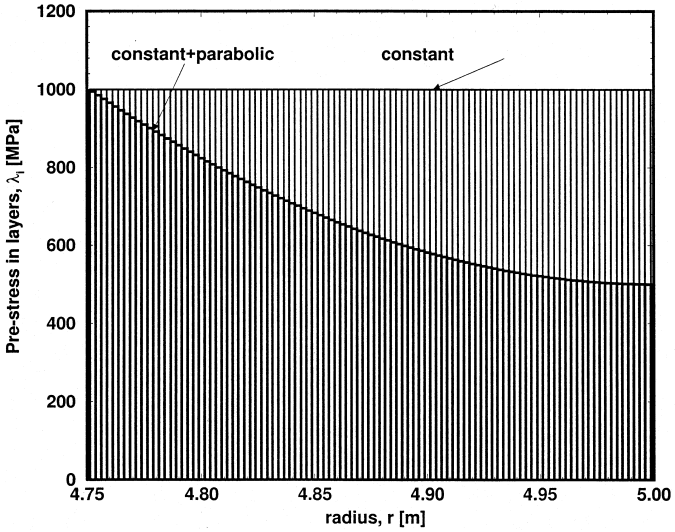

Fig. 5. Distribution of local pre-stress in layers.

Now, consider the other pre-stressing loading case where we apply only the axial forces P_i^z in all the layers. Equations (80) and (81) become

$$\sum_{i=2}^{N}(b_i-a_i)\boldsymbol{S}_{\theta z}^{(i-1)}\boldsymbol{P}^z=0 \tag{93}$$

$$\sum_{i=2}^{N}(b_i^2-a_i^2)\boldsymbol{S}_{zz}^{(i-1)}\boldsymbol{P}^z=0 \tag{94}$$

Again, since the pre-stressing forces can be of any magnitude, it can be concluded that $\boldsymbol{S}_{\theta z}$ and $\boldsymbol{S}_{zz}$ are each singular with one rank deficiency.

3. Residual stresses due to application of known pre-stressing force distribution

For a known distribution of pre-stress forces, the residual stresses in layers can be determined from eqn (54). Simple force distributions such as constant pre-stress or gradually varying pre-stress in layers are easy to apply and are commonly used during fabrication to reduce fiber waviness. Here we consider two such distributions, namely, a constant local self-stress $\lambda_i = 1000$ MPa in the fiber and a combination of constant and parabolic self-stress distribution $\lambda_i = 500 + 500\times(r-b)^2/(a-b)^2$ MPa, as shown in Fig. 5. The magnitudes of the self-stresses used here can be caused by relatively small forces. In order to appreciate the magnitudes, consider the AS4/3501-6 carbon fiber with approximate diameter of 8 μm. A simple calculation shows that a 113 lb force is required to generate the 1000 MPa in a 10,000 fiber tow.

The results presented here are for the fabrication of a composite cylinder having an inner radius $a = 4.75$ m, an outer radius $b = 5$ m and composed of 100 layers of equal thickness which are

Table 1
Properties of AS4/3501-6 carbon/epoxy composite (Daniel and Isahi, 1994)

Property	Magnitude
Axial Young's modulus, E_1	142 GPa
Transverse Young's modulus, E_2	10.3 GPa
Axial shear modulus, G_{12}	7.2 GPa
Transverse shear modulus, G_{23}	3.9 GPa
Axial Poisson's ratio, v_{12}	0.27
Axial tensile strength, F_{1t}	2280 MPa
Transverse tensile strength, F_{2t}	57 MPa
Axial shear strength, F_6	100 MPa
Axial compressive strength, F_{1c}	1440 MPa
Transverse compressive strength, F_{2c}	228 MPa

arranged in a repeating $(0/\pm 60/90_2)$ lay-up. The layers are made of AS4/3501-6 carbon/epoxy composite whose properties are listed in Table 1. The residual stresses due to pre-stress forces are superimposed with the stresses caused by application of a hydrostatic pressure $p_b = 25$ MPa. Such hydrostatic pressure can be realized at a water depth of 2500 m.

The cylinder is laid up on a mandrel during fabrication. The radial and axial stiffness of this mandrel may influence the residual stress distribution. It is economical to use a thin mandrel which has low stiffness, rather than a very thick or reinforced, more rigid mandrel. In view of this, we consider the influence of the mandrel radial stiffness on the residual stress magnitude. For comparison, the stress evaluation was done with three steel mandrels of different thickness, a very compliant 5 cm, an intermediate 15 cm and a very stiff 1 m thick mandrel. The results shown in the figures are for the 5 cm and 1 m thickness; Tables 2 and 3 show comparisons including the 15 cm thickness.

Figures 6 and 7 show the local axial stress distribution in the completed structure for the thin and thick mandrel, respectively, under constant pre-stress and external pressure. Also shown in the graphs are the tensile and compressive stress limits listed in Table 1. The cylinder built on thin mandrel experiences high compressive stresses near the inner surface which gradually decrease towards the outer surface. In the thick mandrel case, the stress distribution through the wall thickness remains almost constant.

The local transverse stress distribution for both mandrel stiffness are shown in Figs 8 and 9. The thin mandrel results indicate that the stresses in the 0 and 90° layers remain almost constant through the thickness. The 60° layer stresses have large variations and they change from compressive stresses near the inner surface to tensile stresses near the outer surface. The stresses near the surfaces exceed strength limits, indicating the possibility of failure. Thick mandrel results show that the stresses are compressive, remain almost constant throughout and do not exceed the strength limits.

The local shear stresses in both mandrel cases appear only in the 60° layers, as shown in Figs 10 and 11. Again, the thin mandrel shear stress exceeds the limits near the two surfaces while the thick mandrel results stay within the strength bounds. Therefore, the results for constant pre-stress indicate that the cylinder made with a rigid mandrel can support a relatively higher magnitude of pre-stress.

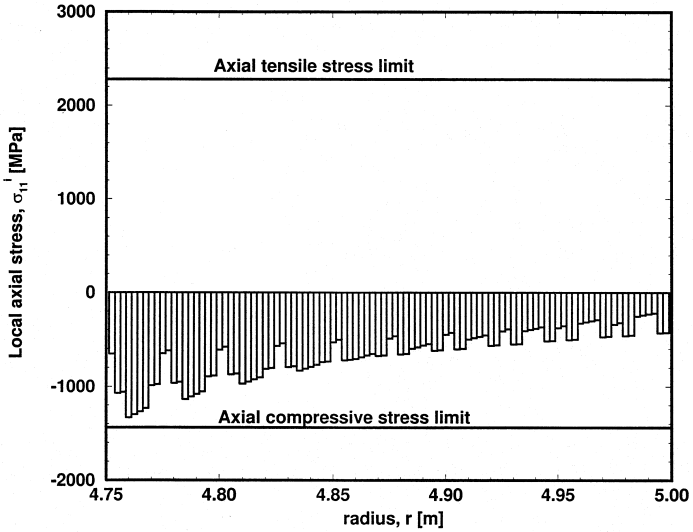

Fig. 6. Local axial stresses due to constant pre-stress of Fig. 5 and external pressure $p_b = 25$ MPa; mandrel thickness 5 cm.

The local axial stress distribution under a combination of constant and parabolic pre-stress, Fig. 5, for thin and thick mandrel stiffness are shown in Figs 12 and 13, respectively. The thin mandrel results show that the compressive stresses are higher in the inner layers, while the thick mandrel results show an opposite trend. The stresses remain within the strength bounds in both cases. The transverse stress distributions shown in Figs 14 and 15 indicate that in both mandrel cases, the

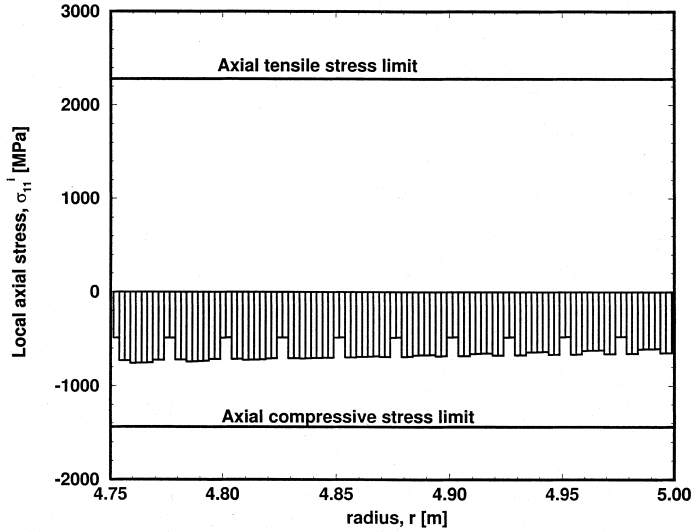

Fig. 7. Local axial stresses due to constant pre-stress of Fig. 5 and external pressure $p_b = 25$ MPa; mandrel thickness 1 cm.

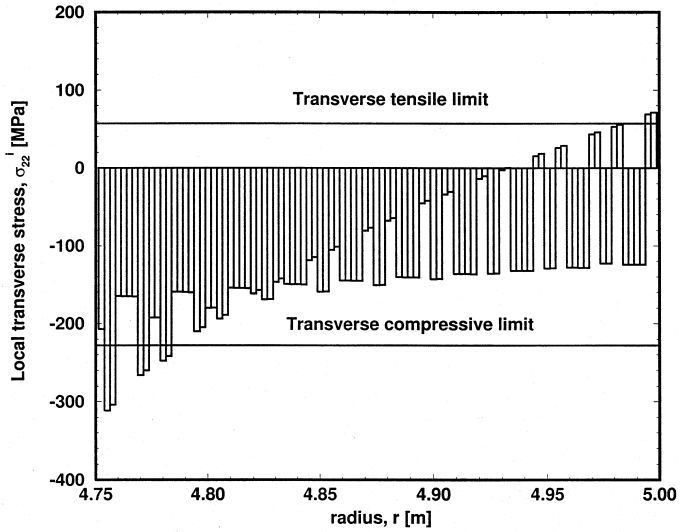

Fig. 8. Local transverse stresses due to constant pre-stress of Fig. 5 and external pressure $p_b = 25$ MPa; mandrel thickness 5 cm.

stresses in 0 and 90° layers remain constant while the 60° layer stresses show a variation. The thin mandrel cylinder experiences higher compression near the inner surface than the thicker one, but both remain within the strength limits. The shear stress distribution in Figs 16 and 17 shows that the thick mandrel supports high shear stress near the inner surface exceeding the shear stress limits.

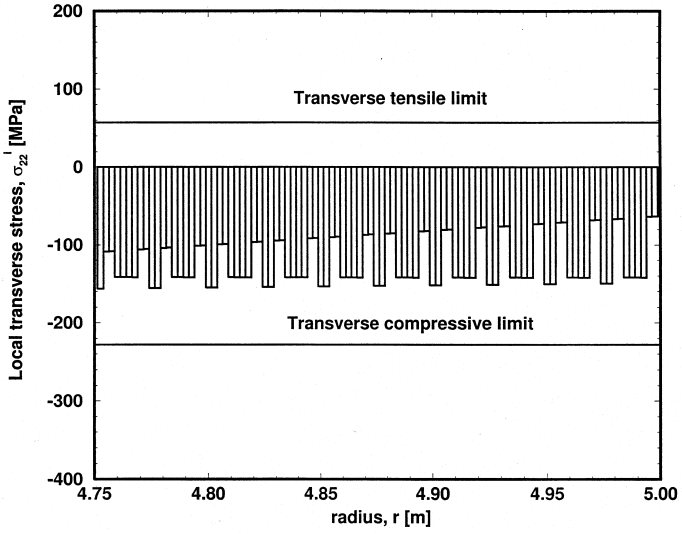

Fig. 9. Local transverse stresses due to constant pre-stress of Fig. 5 and external pressure $p_b = 25$ MPa; mandrel thickness 1 m.

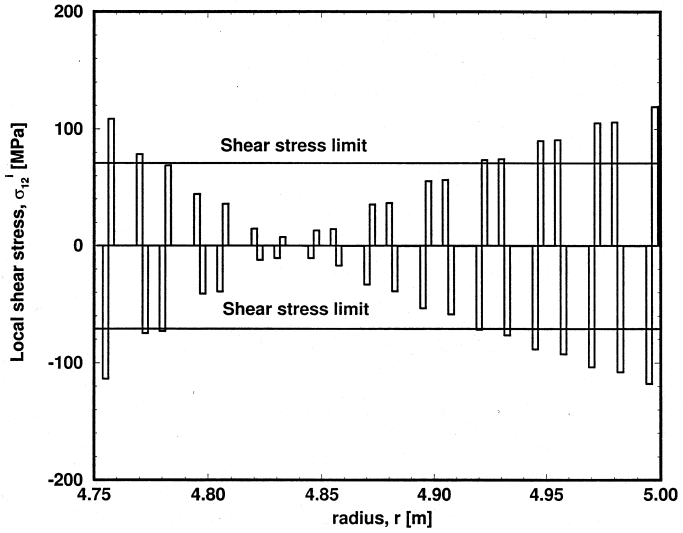

Fig. 10. Local shear stresses due to constant pre-stress of Fig. 5 and external pressure $p_b = 25$ MPa; mandrel thickness 5 cm.

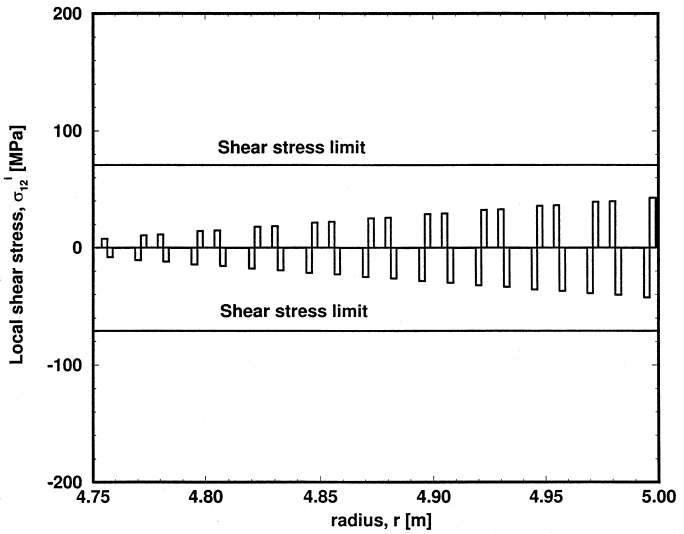

Fig. 11. Local shear stresses due to constant pre-stress of Fig. 5 and external pressure $p_b = 25$ MPa; mandrel thickness 1 m.

Therefore, under combined constant and parabolic distributions, the thin mandrel cylinder can support higher magnitudes of pre-stress than the rigid mandrel cylinder.

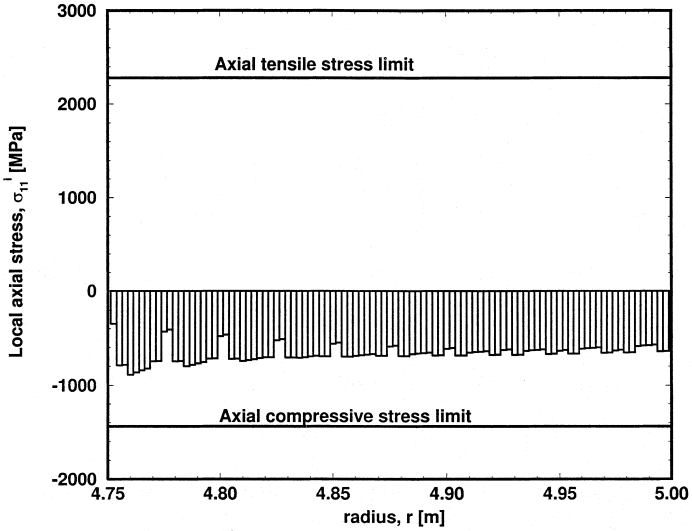

Fig. 12. Local axial stresses due to combined constant and parabolic pre-stress of Fig. 5 and external pressure $p_b = 25$ MPa; mandrel thickness 5 cm.

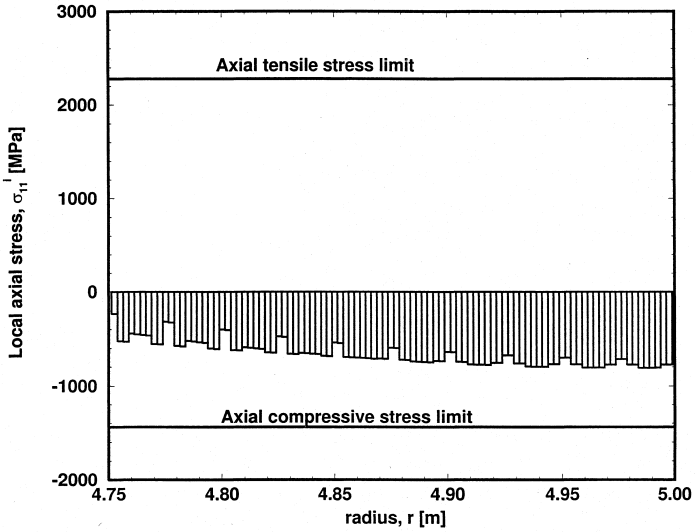

Fig. 13. Local axial stresses due to combined constant and parabolic pre-stress of Fig. 5 and external pressure $p_b = 25$ MPa; mandrel thickness 1 m.

4. Optimal solutions

The design of a fabrication process involves control of the residual stresses within the completed structure such that they are well within the required strength limits. The direct process of applying

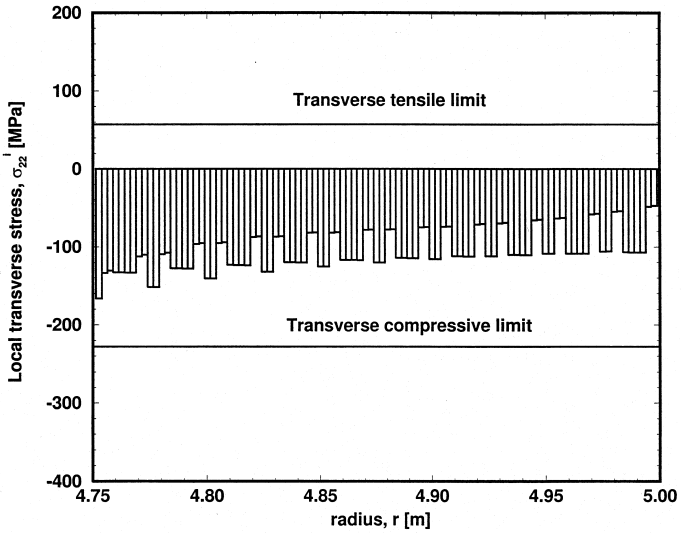

Fig. 14. Local transverse stresses due to combined constant and parabolic pre-stress of Fig. 5 and external pressure $p_b = 25$ MPa; mandrel thickness 5 cm.

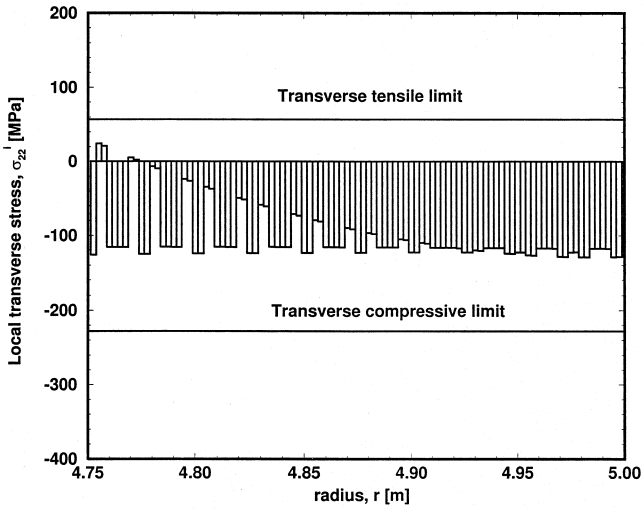

Fig. 15. Local transverse stresses due to combined constant and parabolic pre-stress of Fig. 5 and external pressure $p_b = 25$ MPa; mandrel thickness 1 m.

the known distribution of pre-stressing forces may not always guarantee this. Therefore, we need to determine the distribution of pre-stress in layers to maintain the desired level of residual stresses.

We note that the principal stress components of interest here are the global axial and transverse stresses in layers, which have to be kept within required levels. The solution therefore, involves condition equations representing the stress levels that are large in number than the unknown

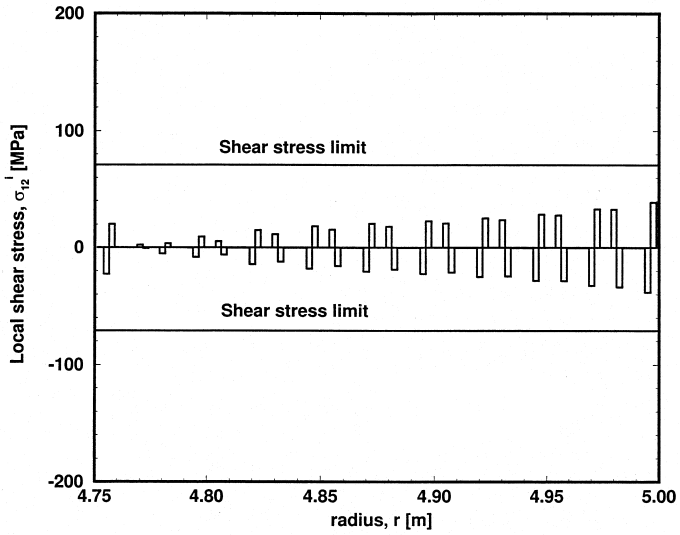

Fig. 16. Local shear stresses due to combined constant and parabolic pre-stress of Fig. 5 and external pressure $p_b = 25$ MPa; mandrel thickness 5 cm.

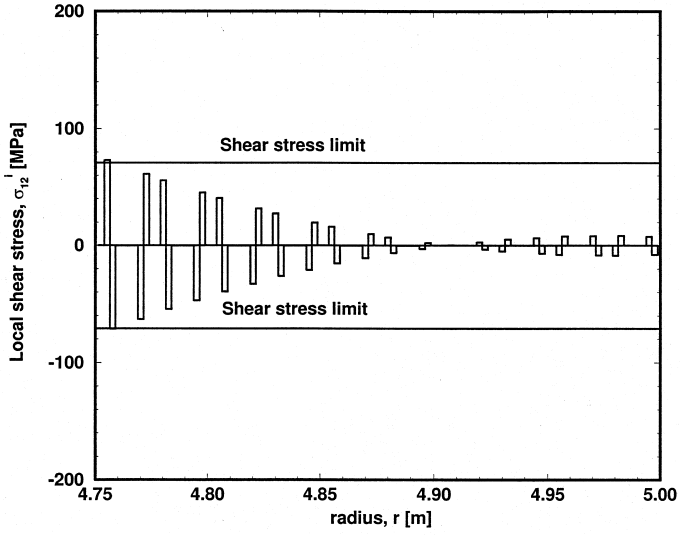

Fig. 17. Local shear stresses due to combined constant and parabolic pre-stress of Fig. 5 and external pressure $p_b = 25$ MPa; mandrel thickness 1 m.

variables which are the pre-stress forces. We seek an optimal solution for the forces that yield desired distributions of stresses in layers.

The objective is to keep the residual stresses in all the layers at minimum. The optimization problem is the minimization of an objective function involving the stress variance defined by,

$$I = \sum_{i=2}^{N} [(\sigma_{\theta\theta}^i)^2 + (\sigma_{zz}^i)^2] \rightarrow \text{minimum} \tag{95}$$

Certain constraint conditions are imposed on the solution. Only tensile pre-stressing forces can be applied in the layers and therefore we have,

$$P_i \geqslant 0 \tag{96}$$

Further, the residual stresses caused in the layers should not exceed the strength limits. A maximum stress failure criterion for predicting strength limits, imposes additional constraints on the residual stresses. The hoop stress $\sigma_{\theta\theta}^i$ and the axial stress σ_{zz}^i in the global system can be resolved along the principal material axes and equated to the corresponding axial and transverse strengths as

$$-F_{1c}^i < \frac{\sigma_{\theta\theta}^i + \sigma_{zz}^i}{2} - \frac{\sigma_{\theta\theta}^i - \sigma_{zz}^i}{2}\cos 2\psi_i < F_{1t}^i \quad i = 2, 3, \ldots, N \tag{97}$$

$$-F_{2c}^i < \frac{\sigma_{\theta\theta}^i + \sigma_{zz}^i}{2} + \frac{\sigma_{\theta\theta}^i - \sigma_{zz}^i}{2}\cos 2\psi_i < F_{2t}^i \quad i = 2, 3, \ldots, N \tag{98}$$

$$\left|\frac{\sigma_{\theta\theta}^i - \sigma_{zz}^i}{2}\sin 2\psi_i\right| < F_6^i \quad i = 2, 3, \ldots, N \tag{99}$$

where F_{1t} and F_{1c} are the tensile and compressive strengths in the axial direction, F_{2t} and F_{2c} are the tensile and compressive strengths in the transverse direction, F_6 is the shear strength and ψ_i is the winding angle in the ply (i).

The above optimization problem can be restated in a matrix form more suitable in the numerical solution procedure described later. We first write the residual stresses using relations (54) with (82) as

$$\sigma_{\theta\theta} = (\boldsymbol{S}_{\theta\theta}\boldsymbol{T}_1 + \boldsymbol{S}_{\theta z}\boldsymbol{T}_2)\boldsymbol{P} = \boldsymbol{S}_\theta \boldsymbol{P} \tag{100}$$

$$\boldsymbol{\sigma}_{zz} = (\boldsymbol{S}_{z\theta}\boldsymbol{T}_1 + \boldsymbol{S}_{zz}\boldsymbol{T}_2)\boldsymbol{P} = \boldsymbol{S}_z \boldsymbol{P} \tag{101}$$

Employing the above equations in the objective function (95) yields:

$$I(\boldsymbol{P}) = \boldsymbol{P}^T \boldsymbol{S} \boldsymbol{P} \tag{102}$$

where $\boldsymbol{S} = (\boldsymbol{S}_\theta^T \boldsymbol{S}_\theta + \boldsymbol{S}_z^T \boldsymbol{S}_z)$ is the symmetric and positive definite matrix. Similarly, the constraint conditions (96) and (97)–(99) can be recast as

$$\boldsymbol{l} < \boldsymbol{A} < \boldsymbol{u} \tag{103}$$

where

$$\boldsymbol{l} = [l_2, l_3, \ldots, l_N, -F_{1c}^2, -F_{1c}^3, \ldots, -F_{1c}^N, -F_{2c}^2, -F_{2c}^3, \ldots, -F_{2c}^N, -F_6^2, -F_6^3, \ldots, -F_6^N]^T \tag{104}$$

$$\boldsymbol{u} = [u_2, u_3, \ldots, u_N, F_{1t}^2, F_{1t}^3, \ldots, F_{1t}^N, F_{2t}^2, F_{2t}^3, \ldots, F_{2t}^N, F_6^2, F_6^3, \ldots, F_6^N]^T \tag{105}$$

are $[4(N-1)\times 1]$ vectors containing the lower and upper bound strength values of the layers,

respectively. Here, l_i and u_i, $i = 2, 3, \ldots, N$ are the upper and lower limits on the pre-stress forces P_i. The constraint matrix $\boldsymbol{A}$ is defined as

$$\boldsymbol{A} = \begin{Bmatrix} \boldsymbol{P} \\ \boldsymbol{C} \end{Bmatrix}; \quad \boldsymbol{C} = \begin{bmatrix} \boldsymbol{T}_3 & \boldsymbol{T}_4 \\ \boldsymbol{T}_4 & \boldsymbol{T}_3 \\ \boldsymbol{T}_5 & -\boldsymbol{T}_5 \end{bmatrix} \begin{Bmatrix} \boldsymbol{S}_0\boldsymbol{P} \\ \boldsymbol{S}_z\boldsymbol{P} \end{Bmatrix} \tag{106}$$

where $\boldsymbol{T}_3$, $\boldsymbol{T}_4$ and $\boldsymbol{T}_5$ are the transformation matrices used to transform the stresses from the global system to the local material system. They can be represented as

$$\boldsymbol{T}_3 = \begin{bmatrix} \frac{1}{2}(1-\cos 2\psi_2) & 0 & \ldots & 0 \\ 0 & \frac{1}{2}(1-\cos 2\psi_3) & \ldots & 0 \\ \vdots & \vdots & \ddots & \vdots \\ 0 & 0 & \ldots & \frac{1}{2}(1-\cos 2\psi_N) \end{bmatrix} \tag{107}$$

$$\boldsymbol{T}_4 = \begin{bmatrix} \frac{1}{2}(1+\cos 2\psi_2) & 0 & \ldots & 0 \\ 0 & \frac{1}{2}(1+\cos 2\psi_3) & \ldots & 0 \\ \vdots & \vdots & \ddots & \vdots \\ 0 & 0 & \ldots & \frac{1}{2}(1+\cos 2\psi_N) \end{bmatrix} \tag{108}$$

$$\boldsymbol{T}_5 = \begin{bmatrix} \frac{1}{2}\sin 2\psi_2 & 0 & \ldots & 0 \\ 0 & \frac{1}{2}\sin 2\psi_3 & \ldots & 0 \\ \vdots & \vdots & \ddots & \vdots \\ 0 & 0 & \ldots & \frac{1}{2}\sin 2\psi_N \end{bmatrix} \tag{109}$$

4.1. Nonlinear optimization

A numerical solution to the optimization problem defined by the quadratic objective function (102) and linear inequality constraints (103) can be solved by quadratic programming. The particular quadratic programming adopted here is the active set method described by Gill et al. (1981). It is motivated by the fact that the optimization problem having $(N-1)$ dimensions corresponding to $(N-1)$ variables is reduced in dimensionality due to nonlinear constraints. An active set of constraints that satisfy the equality constraints at any given feasible point is used in solving a subproblem with equality constraints. For a current active set $\boldsymbol{P}^*$ that is known, minimization is the solution of the linear equality constraint problem defined by

$$\underset{\boldsymbol{P}\in\Re^{N-1}}{\text{minimize}}\, I(\boldsymbol{P}) = \frac{1}{2}\boldsymbol{P}^T\boldsymbol{S}\boldsymbol{P} \text{ subject to } \hat{\boldsymbol{A}}\boldsymbol{P} = \hat{\boldsymbol{b}} \tag{110}$$

where $\hat{\boldsymbol{A}}$ is the submatrix of matrix $\boldsymbol{A}$ whose ith row contains the coefficients of the ith active constraint and $\hat{b}$ is the vector containing the upper or the lower bound values that are satisfied by the active constraints at $\boldsymbol{P}^*$.

The necessary conditions for the minimum of the subproblem in (110) are (Gill et al., 1981)

- $\boldsymbol{l} \leqslant \boldsymbol{AP}^* \leqslant \boldsymbol{u}$, with $\hat{\boldsymbol{A}}\boldsymbol{P} = \hat{\boldsymbol{b}}$.
- $\boldsymbol{Z}^T\boldsymbol{g}(\boldsymbol{P}^*) = \boldsymbol{0}$; or, equivalently, $\boldsymbol{g}(\boldsymbol{P}^*) = \hat{\boldsymbol{A}}^T\boldsymbol{\lambda}^*$. Here, $\boldsymbol{g}(\boldsymbol{P}^*) = [\partial I/\partial P_2, \partial I/\partial P_3, \ldots, \partial I/\partial P_N]$ is the gradient vector of the objective function, $\boldsymbol{\lambda}^*$ is the vector of Lagrange multipliers and $\boldsymbol{Z}$ is the nullspace of $\hat{\boldsymbol{A}}$.
- $\lambda_i^* \geqslant 0$, $i = 1, 2, \ldots, t$ where t is the number of active constraints.
- $\boldsymbol{Z}^T\boldsymbol{S}\boldsymbol{Z}$ is positive semi-definite.

A correct active set is not known beforehand and therefore, a working set to be treated as equality constraints is selected from the original problem and iterated to obtain a correct prediction of an active set. These iterations are carried out in the feasible direction throughout until an optimal solution is obtained. Thus, to start with, we need to know the initial feasible point $\boldsymbol{P}_0$, so that the subsequent search $\boldsymbol{P}_k$ at any kth iteration are also feasible.

The solution proceeds in two phases by finding the feasible initial point $\boldsymbol{P}_0$ in the first phase. The estimation is based on the minimization of the sum of infeasibilities in $\boldsymbol{P}$, which is the case of linear programming that is solved by the modified version of the standard Simplex method. The second phase then proceeds iteratively to solve the actual quadratic problem. The procedure after any kth iteration step can be described as follows (Gill et al., 1981):

(1) The convergence criterion for the kth step is checked. The iteration terminates with $\boldsymbol{P}_k$ as a solution, when convergence is satisfied.
(2) The minimization procedure with current working space or by deleting a constraint in the working space is decided. A general principle for the deletion of a constraint is that it is likely to lower the value of the function. The iteration jumps to step (6) if any constraint has to be deleted.
(3) The feasible search direction is computed by performing the following operations:
   - Null space $\boldsymbol{Z}_k$ of the matrix $\hat{\boldsymbol{A}}$ is obtained through TQ factorization (Gill et al., 1981, 1984).
   - New search direction $\boldsymbol{p}_k = \boldsymbol{Z}_k\boldsymbol{p}_z$ is determined after solving a linear set of equations $\boldsymbol{Z}_k^T\boldsymbol{S}\boldsymbol{Z}_k\boldsymbol{p}_z = \boldsymbol{Z}_k^T\boldsymbol{g}_k$.
   - Lagrange multipliers $\boldsymbol{\lambda}_k$ are estimated through $\min_{\boldsymbol{\lambda}} \|\hat{\boldsymbol{A}}\boldsymbol{\lambda} - \boldsymbol{g}_k\|_2^2$.
(4) Maximum feasible steplength $\bar{\alpha}$ along $\boldsymbol{p}_k$ is computed and a positive steplength α_k is determined such that $I(\boldsymbol{P}_k + \alpha_k\boldsymbol{p}_k) < I(\boldsymbol{P}_k)$ and $\alpha_k \leqslant \bar{\alpha}$. The iteration jumps to (7) if $\alpha_k \leqslant \bar{\alpha}$.
(5) A constraint corresponding to α_k is added to the working set and the associated quantities are modified accordingly.
(6) A constraint corresponding to a negative Lagrange multiplier is deleted from the working and the associated quantities are updated. Back to step (1).
(7) Variables are updated and the next iteration is continued.

The results presented in this paper have been obtained using the NAG Fortran library routine (1993).

4.2. Numerical example

The composite cylinder considered here is the same as that described in Section 3. Optimal solutions are obtained under an external pressure $p_b = 25$ MPa. The equilibrium constraint con-

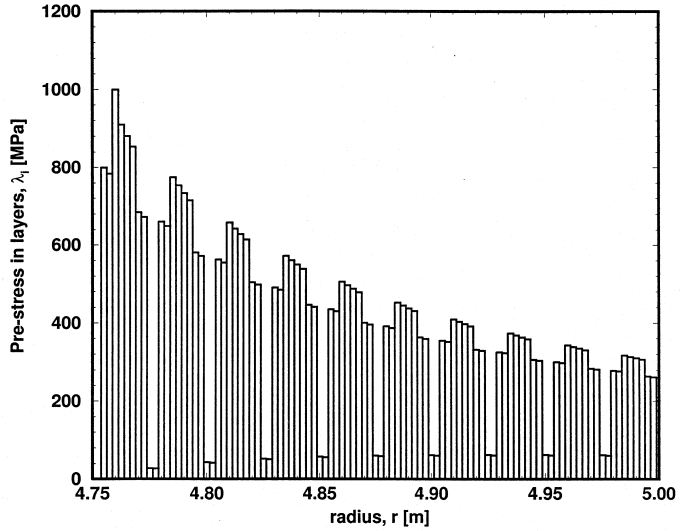

Fig. 18. Optimal pre-stresses in layers, external pressure $p_b = 25$ MPa; mandrel thickness 5 cm.

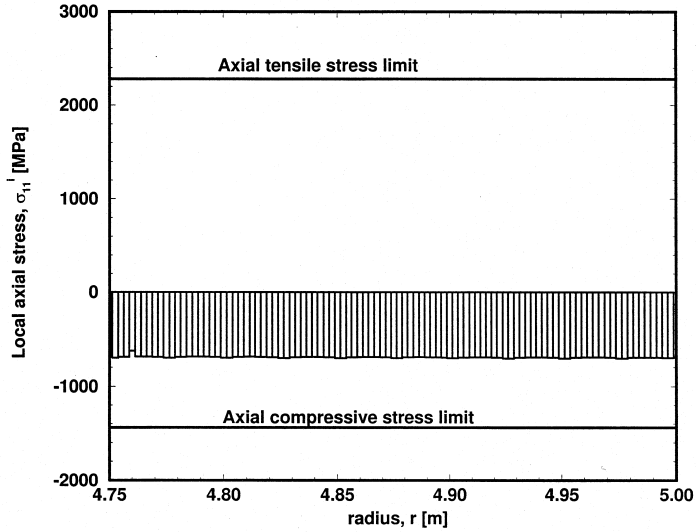

Fig. 19. Local axial stress due to optical pre-stress and external pressure $p_b = 25$ MPa; mandrel thickness 5 cm.

dition indicates that the stress influence matrices are singular with one rank deficiency, hence a free pre-stress $\lambda_5 = 1000$ MPa is introduced in the fifth layer.

Figure 18 shows the local self-stress distribution for optimal pre-stress in a cylinder fabricated with 5 cm mandrel. The self-stress distributions in 60 and 90° layers follow a combination of constant and parabolic types, while the 0° layers admit negligible self-stresses. The corresponding residual stresses in layers are shown in Figs 19–21 along with their strength limits. As required by

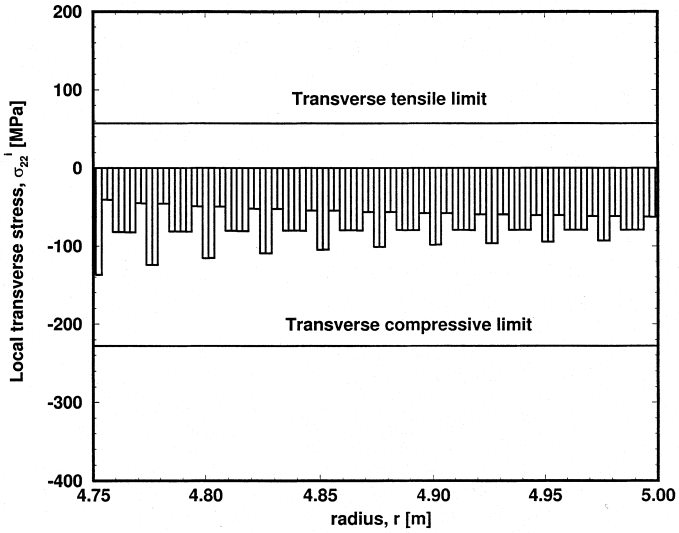

Fig. 20. Local transverse stress due to optimal pre-stress and external pressure $p_b = 25$ MPa; mandrel thickness 5 cm.

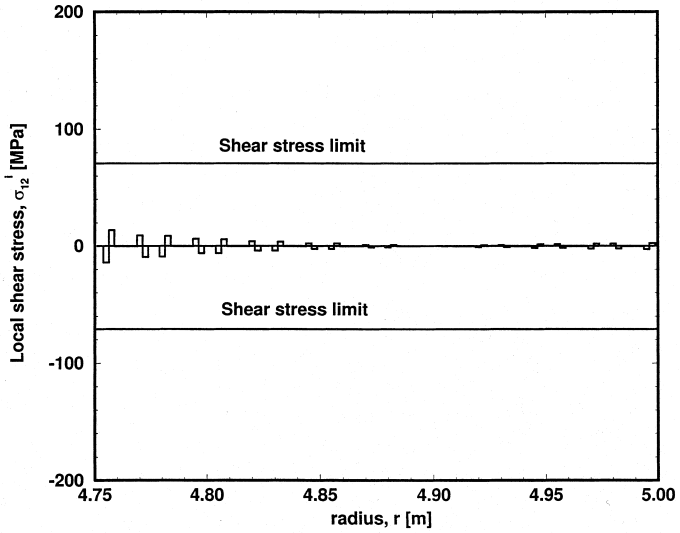

Fig. 21. Shear stress due to optimal pre-stress and external pressure $p_b = 25$ MPa; mandrel thickness 5 cm.

the constraint conditions, the axial, transverse and shear components of residual stresses in all the layers are well within the strength limits. The optimal local pre-stress distribution in the thick mandrel (1 m) cylinder is shown in Fig. 22.

Table 2 and 3 summarize the high and low magnitudes of the ply stresses, in local coordinates of each ply, for the three mandrel thicknesses, under different loading conditions. Table 2 presents the stresses due to application of the external pressure $p_b = 25$ MPa and the constant and combined

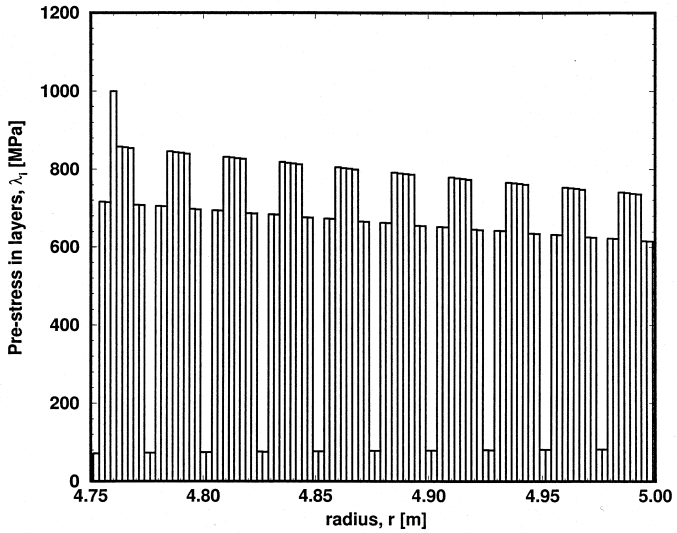

Fig. 22. Optimal pre-stresses in layers, external pressure $p_b = 25$ MPa; mandrel thickness 1 m.

constant and parabolic pre-stress distributions of Fig. 5. Table 3 shows the magnitudes of the same local stresses generated by a superposition of the optimal fiber pre-stress with the external pressure of 25 MPa and also the magnitudes of the local residual stresses caused by the optimized pre-stress acting alone, without the external pressure.

The results indicate that for a given pre-stress profile, a stiffer mandrel will create a more uniform residual and total stresses through the wall thickness. For the optimized pre-stress, the mandrel thickness has less significant influence on the residual stress state, but the required profile is more uniform for a thick mandrel, Figs 18 and 22. Note that other than the 1000 MPa choice of initial pre-stress would produce different residual and total stresses in the structure. The same is true for different choices of ply strengths than those shown in Table 1.

5. Closure

As in our earlier paper (Dvorak and Prochazka, 1996), the principal conclusion reached from the theory and illustrative examples is that fiber pre-stress may cause either beneficial or detrimental residual stress distributions in laminated cylinder structures. Even rather moderate pre-stressing forces may produce residual stress magnitudes that are comparable to those caused by external tractions. In addition, significant thermal residual stresses may be caused in structural parts or samples exposed to uniform temperature changes induced by cooling of the entire structure from the curing temperature. Therefore, careful modeling and analysis of the fabrication process should be an essential part of design procedures for laminated composite structures. The specific problems solved herein illustrate some of the basic rules that should be followed. Use of rather stiff mandrels and gradual reduction of the ply pre-stress forces through the wall thickness are among the most

Table 2
Maximum and minimum stresses due to external pressure of 25 MPa and application of constant and combined constant and parabolic pre-stress distributions of Fig. 5

			Mandrel thickness $t_1 = 5$ cm	Mandrel thickness $t_1 = 15$ cm	Mandrel thickness $t_1 = 1$ m
Local axial stress $i\sigma^i_{11}$ (MPa)	Constant pre-stress[1]	Max	−218.39[2]	−419.41	−476.18[3]
		Min	−1073.40[2]	−987.09	−759.35[3]
	Constant + parabolic pre-stress[1]	Max	−345.84[8]	−264.73	−229.86[9]
		Min	−888.52[8]	−726.73	−808.69[9]
Local transverse stress σ^i_{22} (MPa)	Constant pre-stress[1]	Max	71.35[4]	−2.84	−63.20[5]
		Min	−311.35[4]	−185.37	−156.50[5]
	Constant + parabolic pre-stress	Max	−47.14[10]	−34.10	24.10[11]
		Min	−166.28[10]	−140.94	−129.32[11]
Local shear stress σ^i_{12} (MPa)	Constant pre-stress[1]	Max	119.21[6]	78.83	42.75[7]
		Min	−117.73[6]	−77.86	−42.39[7]
	Constant + parabolic pre-stress[1]	Max	38.97[12]	37.02	73.06[13]
		Min	−38.24[12]	−36.54	−71.27[13]

[1]Fig. 5. [2]Fig. 6. [3]Fig. 7. [4]Fig. 8. [5]Fig. 9. [6]Fig. 10. [7]Fig. 11. [8]Fig. 12. [9]Fig. 13. [10]Fig. 14. [11]Fig. 15. [12]Fig. 16. [13]Fig. 17.

Table 3
Maximum and minimum stresses due to application of optimal fibre pre-stress

			Mandrel thickness $t_1 = 5$ cm	Mandrel thickness $t_1 = 15$ cm	Mandrel thickness $t_1 = 1$ m
Local axial stress σ^i_{11} (MPa)	With external pressure $p_b = 25$ MPa	Max	−624.13[1]	−583.64	−539.60
		Min	−704.55[1]	−704.98	−705.24
	Without external pressure $p_b = 0$	Max	71.87	112.36	156.40
		Min	−0.87	−1.19	−1.27
Local transverse stress σ^i_{22} (MPa)	With external pressure $p_b = 25$ MPa	Max	−40.63[2]	−42.79	−44.82
		Min	−137.12[2]	−131.30	−127.23
	Without external pressure $p_b = 0$	Max	23.54	21.38	19.35
		Min	−72.96	−67.13	−63.07
Local shear stress σ^i_{12} (MPa)	With external pressure $p_b = 25$ MPa	Max	13.77[3]	10.08	6.82
		Min	−14.14[3]	−10.17	−6.87
	Without external pressure $p_b = 0$	Max	13.32	9.62	6.36
		Min	−13.65	−9.69	−6.38

[1]Fig. 19. [2]Fig. 20. [3]Fig. 21.

desirable design features. Of course, specific models and solutions are needed for each material system, fabrication method and structural application.

Acknowledgement

This work was supported by the Ship Structures and Systems S&T Division of the Office of Naval Research; Dr Yapa D. S. Rajapakse served as program monitor.

References

Daniel, I.M., Isahi, O., 1994. Engineering Mechanics of Composite Materials. Oxford University Press, New York.
Dvorak, G.J. Prochazka, P., 1996. Thick-walled composite cylinders with optimal fiber pre-stress. Composites, Part B 27B, 643–649.
Dvorak G.J., Srinivas, M.V., Prochazka, P., 1999. Design and fabrication of submerged cylindrical laminates—I. Int. J. Solids Structures 36, 3917–3943.
Gill, P.E., Murray, W., Wright, M.H., 1981. Practical Optimization. Academic Press, New York.
Gill, P.E., Murray, W., Saunders, M.A., Wrights, M.H., 1984. Procedures for optimization problems with a mixture of bounds and general linear constraints. ACM Transactions on Mathematical Software 10, 282–298.
NAG Fortran Library Manual, 1993. NAG Ltd, Oxford.